RESEARCH ARTICLE

The lncRNA *Hand2os1*/*Uph* locus orchestrates heart development through regulation of precise expression of *Hand2*

Xue Han[1],[*], Jiejie Zhang[2],[*], Yaxi Liu[2],[*], Xiaoying Fan[3], Shanshan Ai[2], Yingjie Luo[2], Xin Li[2], Hengwei Jin[4], Sai Luo[1],[‡], Hui Zheng[1], Yanzhu Yue[2], Zai Chang[1], Zhongzhou Yang[4], Fuchou Tang[3], Aibin He[2],[§] and Xiaohua Shen[1],[§]

ABSTRACT

Exploration and dissection of potential actions and effects of long noncoding RNA (lncRNA) in animals remain challenging. Here, using multiple knockout mouse models and single cell RNA sequencing, we demonstrate that the divergent lncRNA *Hand2os1*/*Uph* has a key complex modulatory effect on the expression of its neighboring gene *HAND2* and subsequently on heart development and function. Short deletion of the *Hand2os1* promoter in mouse diminishes *Hand2os1* transcription to ∼8-32%, but fails to affect *HAND2* expression and yields no discernable heart phenotypes. Interestingly, full-length deletion of *Hand2os1* in mouse causes moderate yet prevalent upregulation of *HAND2* in hundreds of cardiac cells, leading to profound biological consequences, including dysregulated cardiac gene programs, congenital heart defects and perinatal lethality. We propose that the *Hand2os1* locus dampens *HAND2* expression to restrain cardiomyocyte proliferation, thereby orchestrating a balanced development of cardiac cell lineages. This study highlights the regulatory complexity of the lncRNA *Hand2os1* on *HAND2* expression, emphasizing the need for complementary genetic and single cell approaches to delineate the function and primary molecular effects of an lncRNA in animals.

KEY WORDS: lncRNA, *Hand2os1*, *Hand2*, Knockout mice, Single cell transcriptomic analysis, Heart development

INTRODUCTION

Long noncoding RNAs (lncRNAs) have been implicated as an important layer of regulatory information in fine-tuning the spatiotemporal expression of pleiotropic developmental loci in their chromatin neighborhood, thereby modulating cell fate determination in various biological processes (Han et al., 2018; Luo et al., 2016; Morris and Mattick, 2014; Pauli et al., 2011; Ponjavic et al., 2009; Yin et al., 2015). Heart formation is tightly regulated during mouse embryogenesis and involves restriction of

[1]Tsinghua Center for Life Sciences, School of Medicine, and School of Life Sciences, Tsinghua University, Beijing 100084, China. [2]Peking Center for Life Sciences, Institute of Molecular Medicine, Beijing Key Laboratory of Cardiometabolic Molecular Medicine, Peking University, Beijing 100871, China. [3]Beijing Advanced Innovation Center for Genomics, College of Life Sciences, Peking University, Beijing 100871, China. [4]Model Animal Research Center, Nanjing University, Nanjing 210061, China.
*These authors contributed equally to this work
‡Present address: Program in Cellular and Molecular Medicine, Boston Children's Hospital; Department of Genetics, Harvard Medical School, Boston, MA 02115, USA.

§Authors for correspondence (ahe@pku.edu.cn; xshen@tsinghua.edu.cn)

H.Z., 0000-0001-8947-8091; A.H., 0000-0002-3489-2305; X.S., 0000-0002-4590-1502

mesodermal precursor cells to the cardiac lineage and the subsequent formation of a primitive heart tube, which, in turn, undergoes: looping; formation of the outflow tract and atrial and ventricular cavities; and septation to form the mature four-chambered heart (Bruneau, 2008; Olson and Schneider, 2003). Proper commitment of cardiac lineages during this complex process is required for normal development and function of the heart (Brade et al., 2013). Several lncRNAs have been reported to have roles in regulating heart development and function. For example, depletion of *Chast/Wisper* and overexpression of *Mhrt*, *Tincr* or *Carel* protected the heart from hypertrophy in response to pressure overload following transverse aortic constriction surgery (Cai et al., 2018; Han et al., 2014b; Micheletti et al., 2017; Shao et al., 2017; Viereck et al., 2016). Inhibition of *Fendrr* led to embryonic lethality around E13.5 with cardiac hypoplasia (Grote et al., 2013).

The lncRNA *Hand2os1* (also named *Uph* or *lncHand2*) is divergently positioned at −123 bp upstream of the transcription start site (TSS) of *HAND2* (Anderson et al., 2016; Wang et al., 2018). (Throughout this paper, we use the non-standard style of *HAND2*, etc. to distinguish it from the lncRNA.) HAND2, a transcription factor that promotes ventricular cardiomyocyte expansion and cardiac reprogramming, is a crucial regulator of embryonic heart development (McFadden et al., 2005; Song et al., 2012; Srivastava et al., 1997). Cardiac expression of *HAND2* is initially detected in the cardiac crescent at E7.75, continues throughout the linear heart tube at E8.5, is specifically enhanced in the developing right ventricle (RV) and outflow tract (OFT) until E9.5-E10.0, and is downregulated in the cardiac mesoderm but maintained in the neural crest-derived aortic arch arteries (Srivastava et al., 1997; Tamura et al., 2014).

Precise expression of *HAND2* is essential for normal heart morphogenesis and function. It is tightly regulated at the transcriptional level by a network of cardiac transcription factors and upstream enhancers, and at the post-transcriptional level by microRNAs (Bruneau, 2005; Dirkx et al., 2013; McFadden et al., 2005, 2000; Zhao et al., 2007, 2005). Constitutive *HAND2* knockout (KO) in mice display right ventricle hypoplasia and embryonic lethality at E10.5 (Srivastava et al., 1997). Conditional ablation of *HAND2* in specific sets of cardiac cells leads to embryonic lethality at various stages prior to embryonic day E15.5 (summarized in Table S1) (Holler et al., 2010; Morikawa and Cserjesi, 2008; Morikawa et al., 2007; Tsuchihashi et al., 2011; VanDusen et al., 2014). Overexpression of *HAND2* in transgenic mouse models also leads to heart development defects and malfunctions (Table S1) (Dirkx et al., 2013; Togi et al., 2006).

In a polyA knock-in (KI) mouse model of *Uph*/*Hand2os1* reported previously, termination of transcription by insertion of a triple polyadenylation (polyA) stop sequence into intron 1 of *Uph* (−644 bp upstream of the *HAND2* TSS) abolished *HAND2*

expression and led to failed right ventricle formation and lethality at E10.5, partially phenocopying *HAND2* KO mice (Anderson et al., 2016). It was concluded that transcription of *Uph*/*Hand2os1* is an essential switch for the activation of *HAND2* and the onset of heart morphogenesis (Anderson et al., 2016). However, the functional role of *Hand2os1* transcripts and the *Hand2os1* DNA sequences in the heart remains elusive.

To delineate the role of *Hand2os1* in heart development and function, we generated three deletion alleles of *Hand2os1* in mouse (Han et al., 2018). Full-length deletion of the entire *Hand2os1* sequence (*Hand2os1*^F/F KO) led to dysregulated cardiac gene expression programs, septum lesion, heart hypoplasia and perinatal death, which are reminiscent of congenital heart diseases. A short distal deletion at the 3′ end of the *Hand2os1* locus (*Hand2os1*^D/D KO) caused severe contraction defects in adult heart that progressively worsened with increasing age. By comparison, short deletion of the 5′ promoter and exons of *Hand2os1* (*Hand2os1*^P/P KO) effectively diminished *Hand2os1* expression, but failed to produce discernable heart phenotypes in either embryos or adults. These results indicate that the *Hand2os1* DNA locus primarily controls heart development and function. To our surprise, cardiac expression of *HAND2* was sustained in all three *Hand2os1* KO mouse models we generated, in sharp contrast to the abolished expression of *HAND2* in the *Uph*/*Hand2os1* polyA KI embryos (Anderson et al., 2016). Importantly, single cell transcriptomic analysis revealed subtle yet prevalent upregulation of *HAND2* and concordant global gene expression changes in subsets of cardiac cells of *Hand2os1*^F/F embryos. Altogether, these results illustrate a fine-tuning, yet crucial, role for the lncRNA *Hand2os1* locus in restricting the precise spatial expression of *HAND2*, through which *Hand2os1* modulates cardiac lineage development and heart function. This study reveals the unexpected complexity of lncRNA function *in vivo*, and also emphasizes the usage of complementary genetic and single cell approaches to delineate the primary molecular effects and elucidate physiological functions of an lncRNA in animals.

RESULTS
Hand2os1 transcripts are dispensable for heart development
Hand2os1 and *HAND2* are divergently transcribed from the shared core promoter sequences, and are highly enriched in the heart compared with other tissue types analyzed (Fig. 1A, Fig. S1A,B). Within the heart, *Hand2os1* and *HAND2* exhibit an inverse expression pattern during embryonic heart development and postnatal growth (Fig. S1C). We estimated that the abundance of *Hand2os1* transcripts is ∼15-40 molecules per cell, relatively 7- to 23-fold lower than that of *HAND2* transcripts (Fig. S1C). The DNA sequence of *Hand2os1* is 17 kb in length and encompasses a super-enhancer element, and branchial arch (BA) and cardiac enhancers annotated previously (Fig. 1A) (McFadden et al., 2000; Yanagisawa et al., 2003). In E12.5 embryonic hearts, the *Hand2os1* locus as well as *HAND2* and its downstream regions harbor multiple DNase I hypersensitive sites (DHS, E11.5), and show strong binding signals of active histone H3K4me3 and H3K27ac marks, and RNA polymerase II and master transcription regulators of cardiac development, including GATA4, NKX2-5 and HAND2 (E10.5) itself (Fig. 1A) (He et al., 2014; Laurent et al., 2017; Ye et al., 2015; Yue et al., 2014). This suggests a possible involvement of multiple enhancers in regulating *HAND2* expression.

To remove *Hand2os1* transcription/transcripts with minimal manipulation of the genome, we first generated two mouse models

carrying short genomic deletions at the 5′ or 3′ end of the *Hand2os1* locus, keeping the cardiac and branchial arch enhancers intact (Fig. 1A) (Han et al., 2018). In the 5′ proximal knockout allele (*Hand2os1*^P KO), we deleted a 1 kb DNA sequence covering the core promoter and the first two exons of *Hand2os1* (Fig. 1A) (Han et al., 2018). The deletion starts at −61 bp and −62 bp upstream of the TSSs of *Hand2os1* and *HAND2*, respectively. To avoid any direct effect of promoter alteration on *HAND2* expression, we generated a 3′ distal knockout allele (*Hand2os1*^D KO) by deleting a 2.7 kb DNA sequence that spans exons 4 and 5 of *Hand2os1*, and is located 13 kb upstream of the *HAND2* TSS (Fig. 1A) (Han et al., 2018). Both *Hand2os1*^P/P and *Hand2os1*^D/D mice from heterozygotes crosses were born at the expected Mendelian ratio and had no overt morphological defects in the heart (Fig. 1B, Fig. S1A; data not shown).

Levels of truncated *Hand2os1*^P transcripts lacking exons 1 and 2 were substantially downregulated to ∼10-17% compared with heterozygous and wild-type littermates (Fig. 1C, Fig. S1A). Analysis of pre-mature transcripts using intronic primers suggested residual ∼8-32% of *Hand2os1* transcription remaining in E12.5 embryonic hearts of *Hand2os1*^P/P mice (Fig. S1A,D). *Hand2os1*^P/P KO mice therefore provide a partial loss-of-function model. However, cardiac expression of *HAND2* was not altered in *Hand2os1*^P/P mice (Fig. 1C, Fig. S1A).

Hand2os1^D/D mice expressed a mutant *Hand2os1* RNA that lacks exons 4 and 5 with 67% of its sequence remaining (Fig. S1A). Embryonic expression of *HAND2* in *Hand2os1*^D/D hearts was not affected (data not shown). However, *Hand2os1*^D/D adult cardiomyocytes showed moderate but significant increases of both *Hand2os1* and *HAND2* transcripts (∼53% and ∼34%, respectively) (Fig. 1D). It has been reported that aberrant upregulation of *HAND2* in the postnatal heart contributes to pathological myocardial hypertrophy and heart failure (Dirkx et al., 2013). Interestingly, *Hand2os1*^D/D, but not *Hand2os1*^P/P, mice progressively developed heart contraction defects at 6-10 weeks, with a ∼10-30% decrease in fractional shortening (Fig. 1E; Table S2). Consistently, many genes involved in heart development, cardiac muscle contraction and the cell cycle were dysregulated in *Hand2os1*^D/D cardiomyocytes (Fig. S1E,F; Tables S3 and S4). These results suggest that the *Hand2os1* locus may exert a complex, pleiotropic influence on *HAND2* expression and heart physiology.

Deletion of the entire *Hand2os1* locus causes congenital heart defects and perinatal lethality
Next, to rule out the possibility that residual activities of *Hand2os1* might promote *HAND2* expression and heart morphogenesis in the promoter and distal KO mouse models, we deleted a 17 kb sequence covering the entire *Hand2os1* genomic region to completely eliminate *Hand2os1* expression (Fig. 1A, Fig. S2A) (Han et al., 2018). The deletion starts at −59 bp and −64 bp upstream of *Hand2os1* and *HAND2* TSSs, respectively, and encompasses the super-enhancer and two known enhancers of *HAND2* expression (Fig. 1A). This mutant allele is designated as *Hand2os1* full-length knockout (*Hand2os1*^F KO).

Heterozygous *Hand2os1*^F/+ intercrosses failed to produce viable homozygous offspring (0 out of 77 pups) at the weaning stage (Fig. 2A, Fig. S1A). Viable *Hand2os1*^F/F embryos were observed during mid-gestation at the expected Mendelian frequency until E16.5. *Hand2os1*^F/F newborns became cyanotic and invariably died shortly after birth (Fig. 2B). Gross morphological examination of hearts revealed abnormal blood coagulation and fatal thrombosis in *Hand2os1*^F/F newborns (Fig. 2C). Macroscopically, the most severe
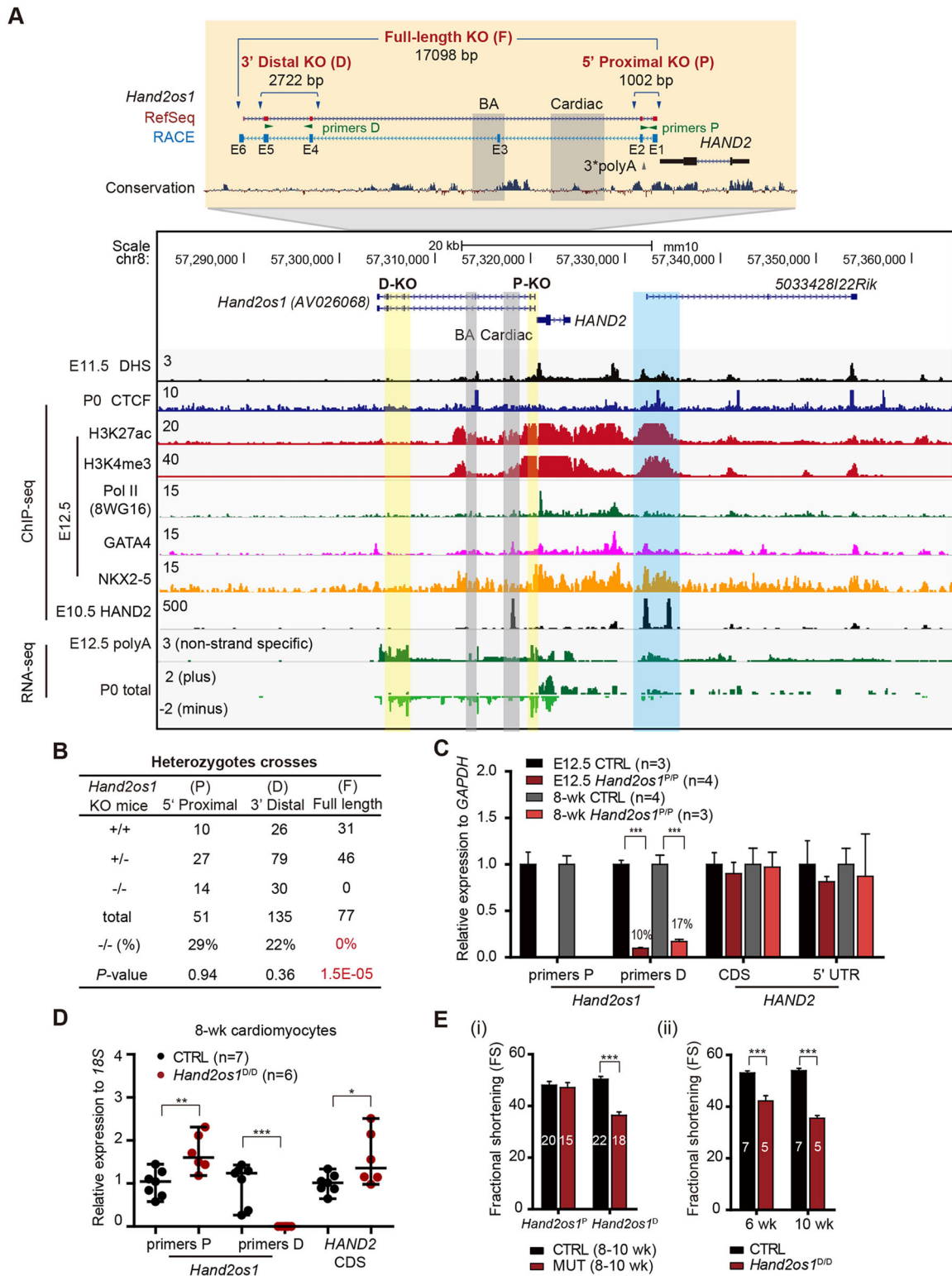
Fig. 1. *Hand2os1* transcripts are dispensable for cardiac development. (A) *Hand2os1* knockout strategies for 5′ proximal KO (P), 3′ distal KO (D) and full-length KO (F) shown in the UCSC genome browser view. The location of the 3*polyA insertion by Anderson et al. is shown, along with the full *Hand2os1* transcript characterized by RACE. Blue arrowheads, sgRNA targeting sites; green arrowheads, RT-qPCR primers; blue shading, putative enhancers; brackets and yellow shading, deleted regions; gray shading, the branchial arch (BA) enhancer and the cardiac enhancer. (B) Survival analysis of *Hand2os1* KO lines. The *P*-values are based on the χ^2 test. (C) RT-qPCR analysis of *Hand2os1* and *HAND2* in E12.5 hearts and 8-week-old cardiomyocytes of *Hand2os1*$^{P/P}$ mice. Data are mean±s.e.m. We estimated ∼2-7 molecules of truncated *Hand2os1*^{P} transcripts per mutant cell, in comparison with ∼15-40 molecules of *Hand2os1* transcripts per wild-type cell (also see Fig. S1C). (D) RT-qPCR analysis of *Hand2os1* and *HAND2* in 8-week-old cardiomyocytes of *Hand2os1*$^{D/D}$ mice. Data are shown as median with range. (E) Echocardiographic measurement of fractional shortening (FS) in *Hand2os1*$^{P/P}$ and *Hand2os1*$^{D/D}$ mice of 8-10 weeks (i), and *Hand2os1*$^{D/D}$ mice at 6 and 10 weeks (the same mice were followed) (ii). Data are mean±s.e.m. (*n* is indicated in each column). In C-E, CTRL indicates the control heterozygote and wild-type littermates; *n*, number of analyzed mice; *P<0.05; **P<0.01; ***P<0.001.

phenotype in homozygous embryonic hearts is the presence of a septum lesion (8 out of 12) (Fig. 2D). Right ventricular (RV) hypoplasia was also frequently observed with significantly decreased chamber volume (10 out of 12) and slightly reduced thickness of the compact myocardium of the right ventricle (3 out of 12) in Hand2os1^F/F mutant hearts (Fig. 2D). These defects are reminiscent of congenital heart diseases and, in combination, may provide a morphological explanation for the heart failure of Hand2os1^F/F mice in response to increased demand for cardiac output and stress at birth (see the Discussion).

Notably, Hand2os1^F/F newborns had cleft palate (Fig. S2B), resembling the craniofacial defects observed in branchial arch enhancer KO mice, which reportedly failed to suckle and died with an empty stomach 24 h after birth (Yanagisawa et al., 2003). As Hand2os1^F/F pups died much earlier, within hours of birth, we reasoned that the suckling defect is not the cause of death in these animals. It has been reported that loss of HAND2 in neural crest lineage mediated by WNT1-Cre led to misalignment of aortic arch arteries and embryonic lethality before E15.5 (Morikawa and Cserjesi, 2008). In comparison, Hand2os1^F/F embryos showed normally developed aortic arch arteries (Fig. S2C), and no gross abnormalities in other organs, including liver and lung (Fig. S2D). Moreover, Hand2os1^F/F pups showed normal floating lungs in a buoyancy test (data not shown), excluding the possibility of respiratory failure as the cause for their immediate death upon birth.

To reveal transcriptional changes that underlie the morphological defects and perinatal lethality, we performed RNA-seq analysis of E11.5 embryonic hearts and E16.5 ventricles isolated from littermates from Hand2os1^F/+ intercrosses. Interestingly, a subset of gene programs pertaining to cardiac muscle contraction, such as ACTA1, COX6C and MYL2, were upregulated in Hand2os1^F/F embryonic hearts at E11.5, implying abnormally increased cardiac myogenesis in the mutant heart (Fig. 2E,F; Tables S3 and S5). Further transcriptome analysis of E16.5 ventricles also revealed significant upregulation of genes related to hypertrophic cardiomyopathy in Hand2os1^F/F embryos (Fig. S2E; Tables S3 and S6). The transcriptomic defects may offer a molecular explanation for heart morphological defects and function failure of Hand2os1^F/F newborns.

Sustained HAND2 expression in Hand2os1^F/F embryos

To study the direct effect of Hand2os1 deletion on HAND2 expression, we first confirmed the complete absence of Hand2os1 transcripts in Hand2os1^F/F mutant embryos by RNA-seq and RT-qPCR (Figs S2A and S3A). No RNA signals were detected downstream of the Hand2os1 locus in Hand2os1^F/F embryos (Fig. S2A), ruling out the possibility that downstream transcription might compensate for the loss of Hand2os1. Thus, Hand2os1^F/F KO mice provided a complete loss-of-function model, in which the transcription, transcripts and DNA sequences of Hand2os1 were simultaneously removed. However, to our surprise, the coding sequence (CDS) of HAND2 showed comparable expression between homozygous and heterozygous littermates throughout heart morphogenesis from E9.5 to E16.5 (Fig. 3A,B). The levels of cardiac HAND2 transcripts were not lost in Hand2os1^F/F mutant embryos, in sharp contrast to the abolished expression of HAND2 in the Uph/Hand2os1 polyA KI embryos (Anderson et al., 2016) (see Discussion).

To confirm this finding, we performed RNA in situ hybridization analysis of E9.5 embryos and found similar distribution and expression patterns of HAND2 mRNA between homozygous and heterozygous littermates (Fig. 3C). Immunostaining analysis in transverse sections of E9.5 embryonic hearts also revealed comparable levels of HAND2 protein in mutant embryos

(Fig. 3D, Fig. S3B). We noted a one- to twofold reduction in HAND2 RNA signals that fall into its 5′ untranslated region (UTR) in Hand2os1^F/F embryonic hearts, despite unchanged expression in the CDS of HAND2 (Fig. 3A, Fig. S3C). 5′ RACE analysis revealed an alternative TSS, 447 bp downstream of the annotated TSS of HAND2 (Fig. S3D). Shortening of the HAND2 5′ UTR might promote translation of HAND2 protein, as demonstrated in cultured cells (Fig. S3E) (Curtis et al., 1995; Leppek et al., 2018). Nevertheless, the overall expression of HAND2 at both the RNA and protein levels was sustained in complete absence of Hand2os1.

The mature four-chamber heart of an E16.5 embryo can be experimentally dissected into distinct compartments, in which HAND2 transcripts can then be analyzed by RT-qPCR. Interestingly, except for right ventricles, HAND2 expression showed a tendency to be upregulated in all other compartments of E16.5 Hand2os1^F/F hearts, compared with those of heterozygous littermates (Fig. 3E, Fig. S3F). In particular, HAND2 expression in the mutants was significantly increased by ∼40% in the septum and ∼24% in the right atrium (Fig. 3E).

### Single cell transcriptomic profiling reveals four cardiac cell types

Sustained and slightly upregulated expression of HAND2 in specific regions of mutant Hand2os1^F/F hearts led us to hypothesize that the Hand2os1 locus might be involved in tuning the spatial expression of HAND2 during heart formation. To reveal subtle alterations that are not readily detectable in population-based analysis due to the averaged expression of mixed cells, we performed high-throughput single cell RNA-seq analysis of E11.5 embryonic hearts isolated from Hand2os1^F/F and wild-type littermates (Fig. 4A). To delineate the primary transcriptional effects of Hand2os1 deletion, we chose to analyze embryos at E11.5, which is also the most convenient early time point that we could experimentally isolate enough cells for 10× Genomics cell sorting and library construction. After removing sequencing reads from hematopoietic cells, we obtained expression profiles for a total of 3600 cardiac cells, including 2108 for Hand2os1^F/F and 1492 for the wild type, with an average of 0.06 million reads/∼13,000 unique molecule identifier (UMI) counts per cell and a median level of 3492 expressed genes per cell [transcripts per million (TPM)>0] (Fig. 4A,B; Table S7).

Classification using the t-distributed stochastic neighbor embedding method (t-SNE) revealed four well-separated clusters of cells that differentially express distinct marker genes (Fig. 4B-D; Tables S7 and S8). About 43% (1550) of cells are cardiomyocytes (CMs) expressing NKX2-5 and MYH7, and ∼31% (1126) are mesenchymal cells (MCs) expressing CTHRC1 and POSTN. About 12% (416) of cells are epicardial cells (EPs) marked by UPK1B and UPK3B, and ∼14% (508) are endothelial cells (ECs) expressing CDH5 and PECAM1 (Fig. 4B,C; Tables S7 and S8) (Li et al., 2016). Interestingly, altered proportions of cardiomyocytes and mesenchymal cells were observed in Hand2os1^F/F embryonic hearts compared with the wild-type littermates (Fig. 4E). Mutant CMs and MCs increased ∼7% and decreased ∼8%, respectively, while ratios of mutant EPs and ECs remained similar (Fig. 4E). Hundreds of single cell profiles obtained for each cell type thus provided large numbers of cells for in-depth statistical comparisons of gene expression changes between mutant and wild-type hearts.

Upregulation of HAND2 and nearby genes in Hand2os1^F/F embryos

HAND2 is ubiquitously expressed (TPM>0) in 60% of cardiac cells at E11.5 (Fig. 5A). This observation was consistent with previous
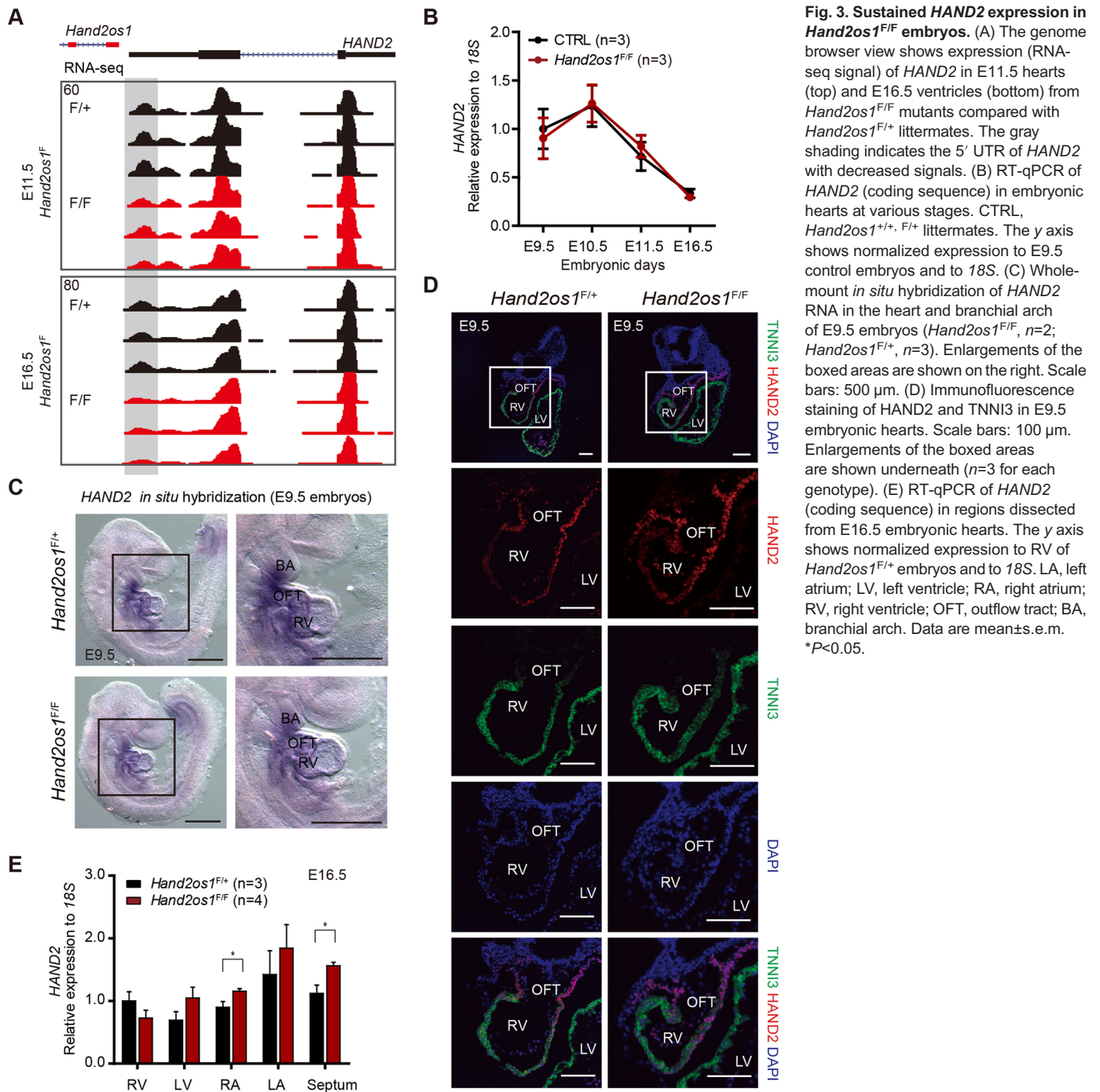
4
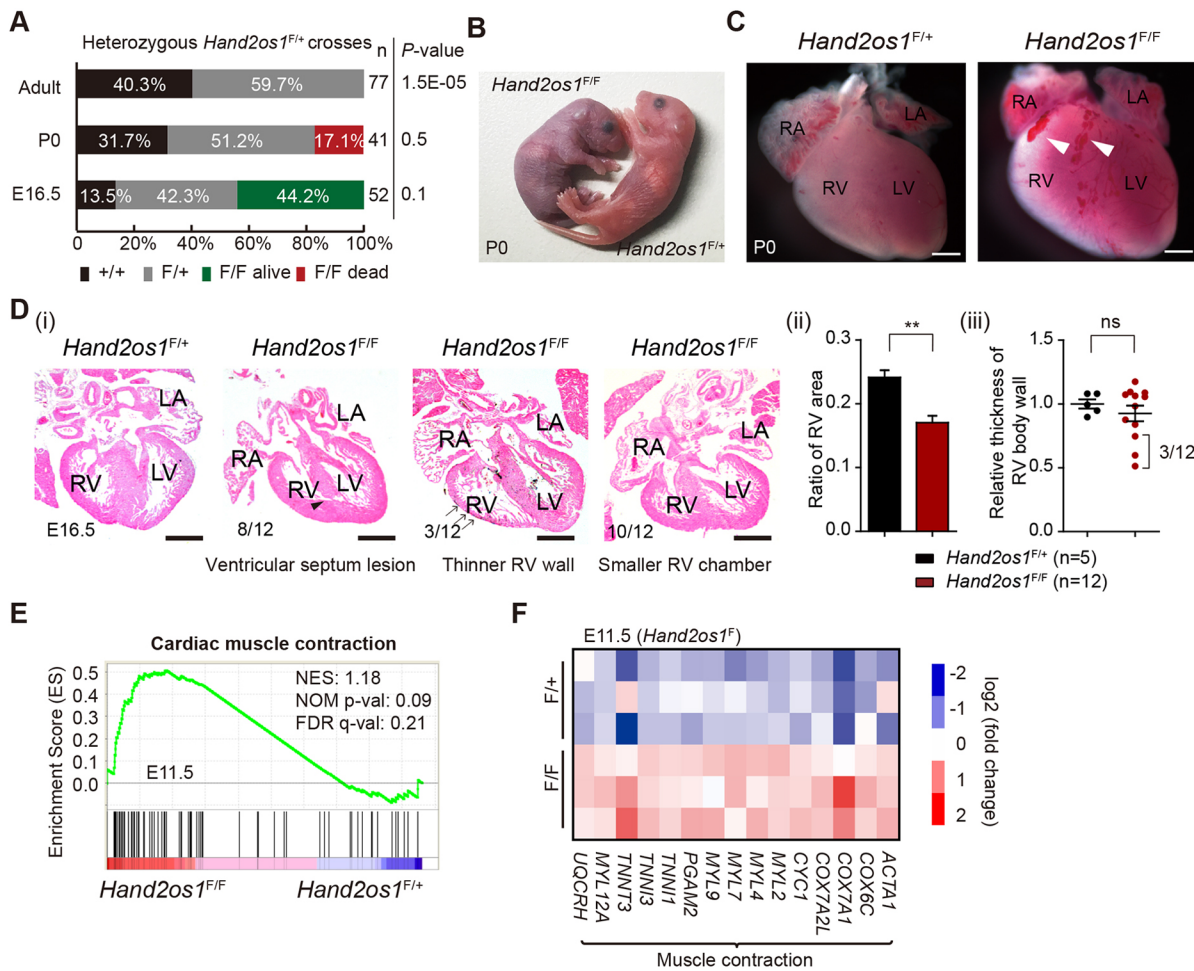
Fig. 2. Deletion of the entire *Hand2os1* locus causes congenital heart defects and perinatal lethality. (A) Survival analysis of *Hand2os1*[F/+] intercrosses. The *P*-values are based on the χ^2 test. (B) *Hand2os1*[F/+] and *Hand2os1*[F/F] newborns. *Hand2os1*[F/F] newborns (*n*=3) turned cyanotic, demonstrating poor circulation compared with the ruddy *Hand2os1*[F/+] newborns (*n*=7). (C) Abnormal blood coagulation and fatal thrombosis (arrowheads) in *Hand2os1*[F/F] (*n*=4) newborn hearts. Scale bars: 500 μm. (D) Hematoxylin and Eosin staining of transverse sections of E16.5 hearts (i), morphometric analysis of the ratio of right ventricle area (normalized to whole ventricle area) (ii) and relative thickness of right ventricle body wall (iii). Numbers shown in the bottom of mutant hearts in (i) indicate the number of hearts with an indicated defect out of the total number of hearts analyzed. Arrowhead indicates ventricular septum lesion. Arrows indicate thinner right ventricular compact myocardium. Scale bars: 500 μm. Data are mean±s.e.m. **P<0.01. (E) Gene set enrichment analysis (GSEA) shows upregulation of genes related to cardiac muscle contraction (KEGG PATHWAY: mmu04260) in *Hand2os1*[F/F] E11.5 hearts. NES, normalized enrichment score. (F) Heatmap of representative genes that are dysregulated in E11.5 hearts of *Hand2os1*[F/F] embryos. RV, right ventricle; LV, left ventricle; RA, right atrium; LA, left atrium.

reports of robust expression of HAND2 detected in many types of cardiac cells using RNA *in situ* hybridization and immunostaining (Laurent et al., 2017; VanDusen and Firulli, 2012). Interestingly, the *Hand2os1*[F/F] hearts appeared to have a 10% increase (from 60% to 70%) of *HAND2*-positive populations (Fig. 5A). The observed increase of mutant CMs mainly resulted from an increase in *HAND2*-positive cardiomyocytes (*P*=2E-04), while the observed decrease of mutant MCs mainly resulted from a decrease of *HAND2*-negative mesenchymal cells (*P*=6E-04) (Fig. 5B). Thus, the opposing changes in the percentages of mutant CMs and MCs appear to be positively correlated with changes of *HAND2* expression in these populations.

Although the overall percentage of ECs and EPs remained the same, the percentages of *HAND2*-positive cells exhibited a significant increase. Thus, cell populations expressing *HAND2* increased ~8-24% in all types of cardiac cell in *Hand2os1*[F/F] mutant hearts, with the most significant gain in the ECs (1.4-fold increase from 59% to 83%, *P*=4E-09) (Fig. 5A). Moreover, the median levels of *HAND2* expression went up significantly by 8-12% across four

cardiac cell types (Fig. 5A). In comparison, other master regulators of cardiac development, such as *GATA6*, *GATA4* and *NKX2-5*, either showed unaltered or decreased expression in particular cardiac cell types (Fig. S4A). These results suggest that the subtle, yet global, upregulation of *HAND2* is unlikely to result from sequencing variations between the wild-type and mutant samples.

Next, we sought to determine whether complete removal of *Hand2os1* might also affect the expression of other nearby genes. High-order chromatin structure analysis by Hi-C in mouse embryonic stem cells (ESCs) (Bonev et al., 2017) showed that the *HAND2* and *Hand2os1* loci reside at the boundary of two topologically associating domains (TADs) (Fig. 5C). This boundary demarcates an upstream gene desert of ~0.65 Mb in length from a downstream gene-rich region. Among 10 genes located within ±1 Mb genomic regions surrounding the TSSs of *Hand2os1* and *HAND2*, we found that six were expressed in at least one type of cardiac cell; four of them exhibited very subtle but statistically significant upregulation in the mutant heart (Fig. 5D,E).

Fig. 3. Sustained *HAND2* expression in *Hand2os1*^F/F embryos. (A) The genome browser view shows expression (RNA-seq signal) of *HAND2* in E11.5 hearts (top) and E16.5 ventricles (bottom) from *Hand2os1*^F/F mutants compared with *Hand2os1*^F/+ littermates. The gray shading indicates the 5′ UTR of *HAND2* with decreased signals. (B) RT-qPCR of *HAND2* (coding sequence) in embryonic hearts at various stages. CTRL, *Hand2os1*^+/+, F/+ littermates. The *y* axis shows normalized expression to E9.5 control embryos and to *18S*. (C) Whole-mount *in situ* hybridization of *HAND2* RNA in the heart and branchial arch of E9.5 embryos (*Hand2os1*^F/F, *n*=2; *Hand2os1*^F/+, *n*=3). Enlargements of the boxed areas are shown on the right. Scale bars: 500 µm. (D) Immunofluorescence staining of HAND2 and TNNI3 in E9.5 embryonic hearts. Scale bars: 100 µm. Enlargements of the boxed areas are shown underneath (*n*=3 for each genotype). (E) RT-qPCR of *HAND2* (coding sequence) in regions dissected from E16.5 embryonic hearts. The *y* axis shows normalized expression to RV of *Hand2os1*^F/+ embryos and to *18S*. LA, left atrium; LV, left ventricle; RA, right atrium; RV, right ventricle; OFT, outflow tract; BA, branchial arch. Data are mean±s.e.m. *P<0.05.

Of the four genes with significantly altered expression, one (*Fbxo8*) lies ~0.75 Mb upstream of *Hand2os1,* and three (*SAP30, 5033428I22Rik* and *HMGB2*) lie within the same TAD immediately downstream of *HAND2* (Fig. 5C). For *SAP30* and *5033428I22Rik*, the numbers of cells expressing these genes were significantly upregulated in subsets of mutant cardiac cells (~9-12% increase of *SAP30*-positive CMs and ECs, *P*<0.002; and ~21% increase of *5033428I22Rik*-positive ECs, *P*=2E-06) (Fig. 5E). *HMGB2* and *FBXO8* were slightly upregulated in transcript abundance in subsets of cardiac cells (*P*≤0.01) (Fig. 5D). For comparison, two ubiquitously expressed genes, *EZH2* and *PSMD1*, showed unaltered expression in both transcript abundance and expression

frequency in the mutant hearts (Fig. S4B). The combined results demonstrate a *cis*-regulatory role for the *Hand2os1* locus in dampening the expression of *HAND2* and several neighboring genes in cardiac cells.

Aberrant cardiac gene programs in *Hand2os1*^F/F embryos

About 197 genes showed altered expression in *Hand2os1*^F/F cardiac cells (see the Materials and Methods; Table S9). Interestingly, gene ontology (GO) analysis of these dysregulated genes showed that non-CM cells (EP, MC and EC) are specifically enriched in functional terms related to cardiac muscle contraction and heart morphogenesis (Fig. 6A; Table S9). In addition, gene set
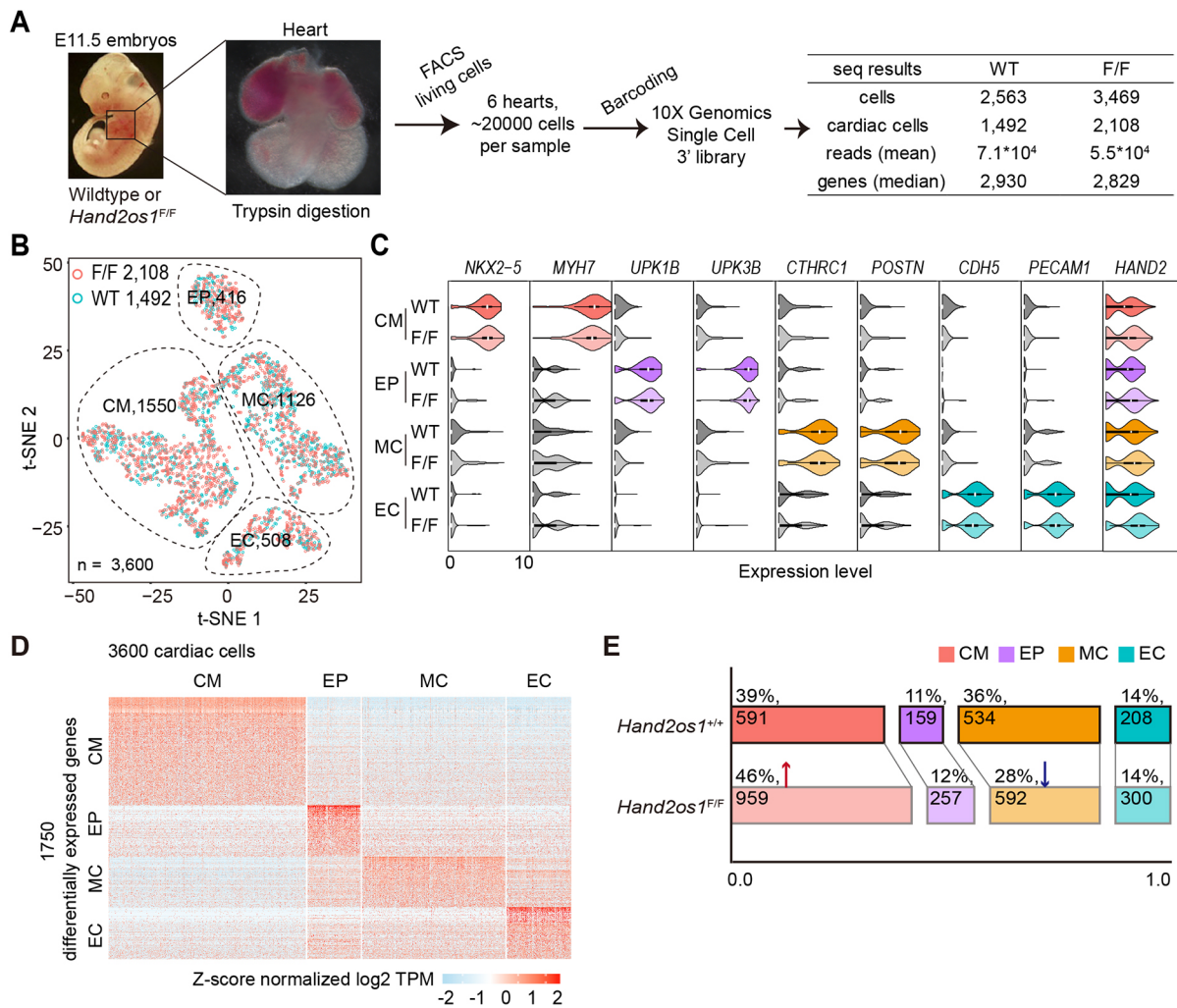
Fig. 4. Single cell transcriptomic profiling reveals four cardiac cell types. (A) Single cell RNA-seq analysis of E11.5 hearts from *Hand2os1*[F/F] and wild-type embryos. (B) Two-dimensional t-SNE visualization of graph-based clustering of 3600 cardiac single cell transcriptomes. CM, cardiomyocyte; EP, epicardial cell; MC, mesenchymal cell; EC, endothelial cell. (C) Violin plots show expression [log2 (TPM/10+1)] of representative marker genes in each cell type. (D) Heatmap shows Z-score normalized expression of differentially expressed genes (1750) in the four cell types shown in B. Rows and columns represent genes and single cells, respectively. (E) Bar charts show distribution of cardiac cells in *Hand2os1*[F/F] and wild-type embryonic hearts. Red arrow, increase of CMs; blue arrow, decrease of MCs. Percentages and cell numbers of each cell type are indicated. TPM, transcripts per million; t-SNE, t-distributed stochastic neighbor embedding.

enrichment analysis (GSEA) showed that non-CMs, but not CMs, of the *Hand2os1*[F/F] mutant exhibit global upregulation of muscle contraction genes and downregulation of genes involved in cardiac septum development (Fig. 6B,C, Fig. S5; Table S3). To directly visualize expression changes, we plotted the ratio of gene expression of *Hand2os1*[F/F] versus control embryos in averaged single cell and bulk RNA-seq of the E11.5 hearts. The heatmap revealed more dramatic expression alterations in mutant non-CMs than in mutant CMs, and the opposing changes in genes related to muscle contraction and cardiac septum development (Fig. 6D).

Many CM marker genes regulating muscle contraction and heart development, such as *MYL4*, *ACTC1*, *TNNC1* and *TNNT2*, were significantly upregulated in their expression levels and frequencies (Fig. 6D,E). In contrast, marker genes enriched in non-CMs, such as *HES1*, *SOX4* and *FZD2*, which are involved in septum development, were specifically downregulated (Fig. 6D,F). For example, ratios of *MYL4*-positive cells in mutant hearts were increased 18-33% in non-CMs (*P*<9E-06), and this was also accompanied by 17-22% increases (*P*<0.0001) of *MYL4* transcript

abundance (Fig. 6E). In comparison, ~9-11% of non-CMs lost *HES1* expression (*P*<0.05) and *HES1* RNA abundance decreased by 12-18% (*P*<0.0001) in mutant hearts (Fig. 6F). These molecular changes corroborate the morphological defects of septum lesion and ventricle hypoplasia observed in *Hand2os1*[F/F] embryonic hearts.

Next, we performed correlation analysis to compare the expression similarity of a panel of 1750 differentially expressed genes (Fig. 4D) in each of the four cardiac cell types with those of wild-type CMs. Mutant and wild-type CMs had the highest median levels of correlation coefficient compared with non-CM cells, indicating the robustness of this assay (Fig. 6G). Interestingly, compared with their wild-type counterparts, non-CMs of *Hand2os1*[F/F] embryos showed significantly higher correlations with CMs (Fig. 6G), indicating the resemblance of gene expression programs in cardiomyocytes. Congruent with concurrent upregulation and downregulation of CM and non-CM marker genes, respectively, these results indicate that mutant non-CMs may be aberrantly reprogrammed towards cardiomyocytes, corroborating the global increase of *HAND2* in *Hand2os1*[F/F] embryonic hearts. It was reported that HAND2
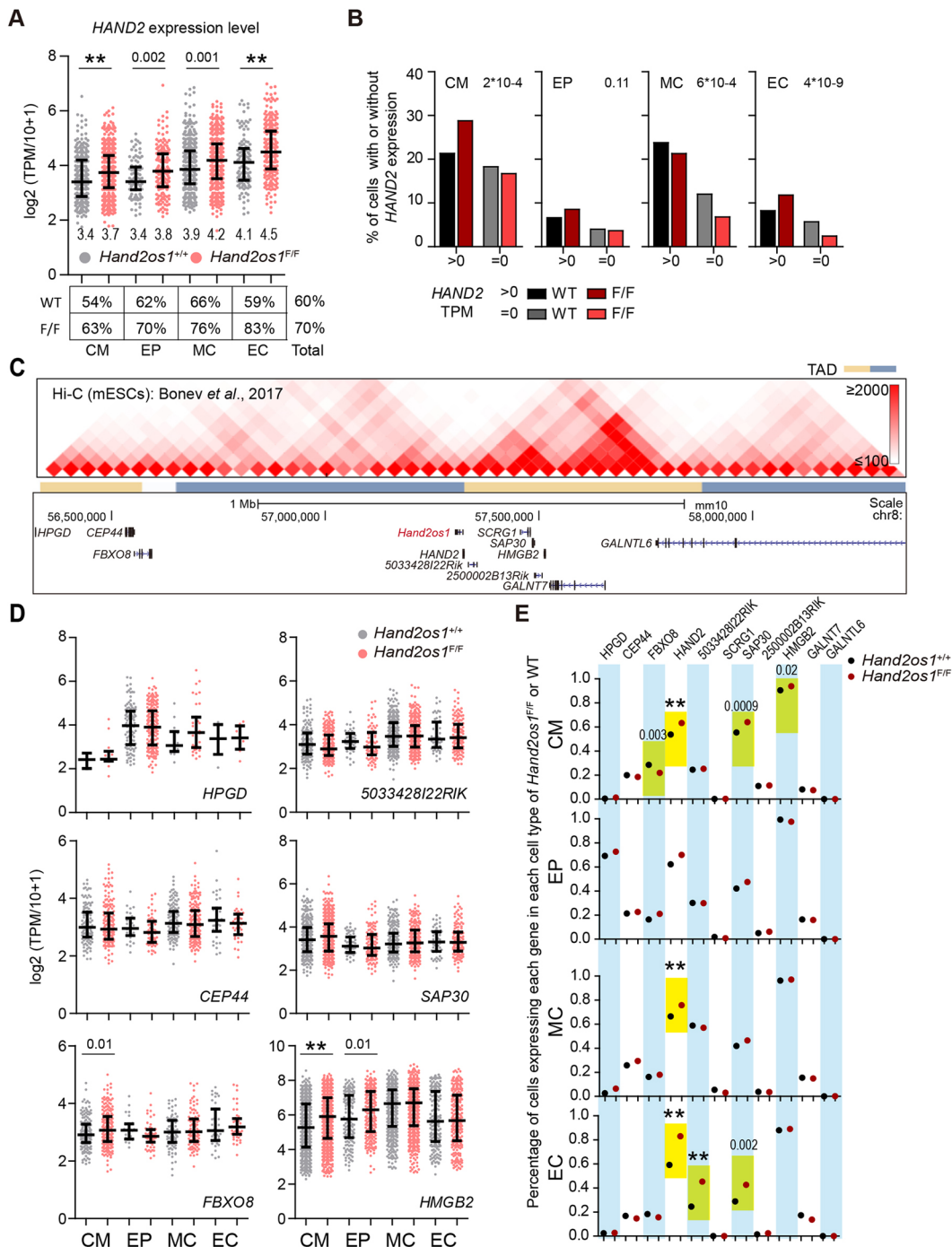
Fig. 5. Upregulation of *HAND2* and nearby genes in *Hand2os1*[F/F] embryos. (A) Scatter plots show expression level and frequency of *HAND2* in four types of cardiac cells from *Hand2os1*[F/F] and wild-type embryonic hearts. The median value is shown at the bottom of each scatter plot. The percentage of *HAND2*-expressing cells (TPM>0) for each cell type is shown under the plot. (B) Correlation of *HAND2* expression and cardiac cell distribution in *Hand2os1*[F/F] and wild-type embryonic hearts. The *y* axis shows the percentage of cells with or without *HAND2* expression in *Hand2os1*[F/F] or wild-type embryonic hearts. The *P*-values for Fisher's exact test are shown at the top. (C) Genome browser of Hi-C data shows TADs within ±1 Mb of the *HAND2* TSS. (D) Scatter plots show expression level of *HAND2*-neighboring genes (in C) with detectable expression. (E) Percentages of cells that express the corresponding gene shown on the top. Yellow highlights significant changes of expression frequency between *Hand2os1*[F/F] and wild-type cells. Scatter plots are shown with median and interquartile range. $0.0001 < P < 0.05$ values are indicated; **$P < 0.0001$.

facilitates cardiomyocyte proliferation and the reprogramming of fibroblasts into functional cardiac-like myocytes *in vitro* and *in vivo* (Song et al., 2012). We conjecture that broad changes in cardiac gene expression are likely to be secondary to altered expression of *HAND2* in *Hand2os1*[F/F] mutant hearts (see the Discussion).

The *HAND2* promoter interacts with downstream enhancers in *Hand2os1*[F/F] embryonic hearts

Enhancer redundancy is commonly observed for the expression of essential developmental genes, and may provide phenotypic robustness in mammalian development (Osterwalder et al., 2018). Dysregulated expression of *HAND2* in *HAND2os1*[F/F] embryonic
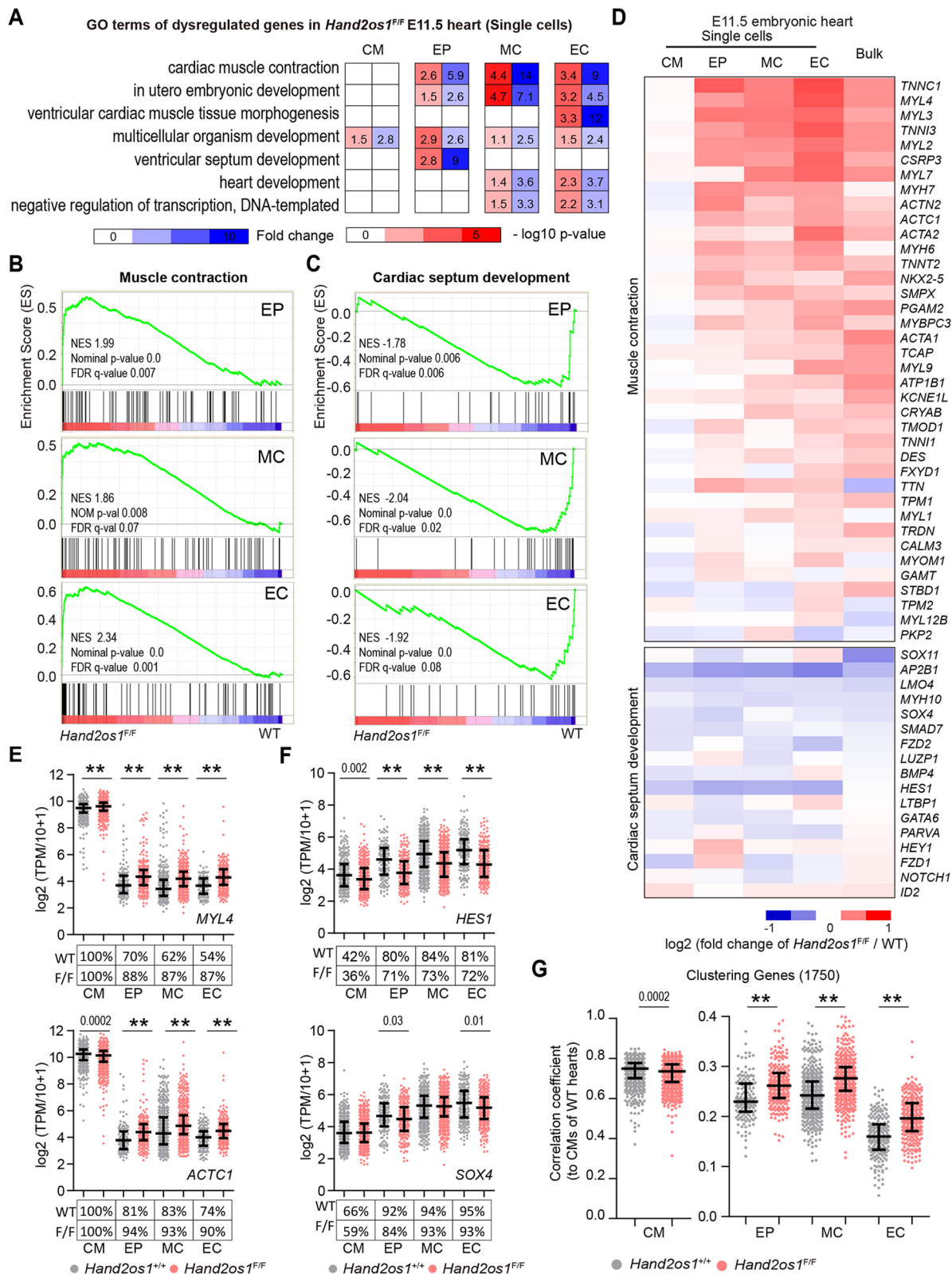
Fig. 6. Aberrant cardiac gene programs in *Hand2os1*^{F/F} embryos. (A) Heatmap shows enriched GO terms (*P*<0.01, at least five genes) of dysregulated genes in each cell type. (B,C) GSEA analysis of genes related to muscle contraction (GO: 0006936) (B) and cardiac septum development (GO: 0003279) (C) in non-CMs (EPs, MCs and ECs). (D) Heatmap shows fold change of representative genes involved in muscle contraction and cardiac septum development in E11.5 hearts of *Hand2os1*^{F/F} compared with wild type. For single cell RNA-seq, fold change of averaged gene expression in each cell is shown. For bulk RNA-seq, fold change of averaged gene expression from replicates (*n*=3 for each genotype) is shown. (E,F) Scatter plots show expression level and frequency of *MYL4* and *ACTC1* (E), and *HES1* and *SOX4* (F). (G) Scatter plots show the Pearson correlation coefficient for each cell when single cell gene expression profiles were compared with the averaged gene expression profile (of 1750 differentially expressed genes shown in Fig. 4D) of wild-type CMs. Scatter plots are shown with median and interquartile range indicated. 0.0001<*P*<0.05 values are indicated; **P<0.0001.

hearts led us to examine possible use of alternative enhancers to sustain *HAND2* expression. We first analyzed the published data of HiCap, a genome-wide promoter-capture method to detect chromatin contacts generated in mouse ESCs (Sahlén et al., 2015). In ESCs, the *HAND2* promoter interacts with two known upstream enhancers (BA and cardiac) in the *Hand2os1* locus, and also with multiple downstream DNA elements embedded in the lncRNA *5033428I22Rik* locus (a strong interaction within the first intron of *5033428I22Rik* is marked by blue shading in Fig. 7).

Next, we performed chromosome conformation capture (3C) in hearts from E16.5 wild-type and mutant embryos. Using the TSS of *HAND2* as the anchor, we analyzed chromatin interactions across its downstream 20 kb region to the first intron of *5033428I22Rik*. Indeed, we observed significantly higher interaction frequencies of the *HAND2* TSS with the promoter and 5′ sequences of *5033428I22Rik* relative to the nearby regions in E16.5 embryonic hearts (Fig. 7). These chromatin contacts peak at a CTCF-binding site that is next to a strong HiCap signal detected in ESCs and overlaps with H3K27ac signals in the 5′ end of the first intron of *5033428I22Rik*. Notably, levels of long-range DNA interactions between the *HAND2* TSS and downstream regions are comparable in *Hand2os1*[F/F] and wild-type embryos, which we reasoned might be due to subtle changes in chromatin structure in subpopulations of mutant cardiac cells or the limited sensitivity of 3C, or both. Nevertheless, analysis of chromatin contacts in ESCs and embryos suggested engagement of alternative downstream enhancers with the *HAND2* promoter, in addition to regulatory elements embedded in the *Hand2os1* locus.

DISCUSSION

Compared with extensive reports of lncRNA functions in cell lines, rigorous exploration and dissection of their potential actions and effects in animals are still limited (Li and Chang, 2014). Precise expression of *HAND2* is crucial for heart formation. Transcription of the divergent lncRNA *Hand2os1* is reportedly essential for *HAND2* activation and heart morphogenesis (Anderson et al., 2016). Using three knockout mouse models, we demonstrate a key role of the *Hand2os1* DNA locus in modulating *HAND2* expression

and normal heart development and function. Full-length deletion of *Hand2os1* led to congenital heart defects and perinatal lethality. Importantly, in embryos lacking the entire *Hand2os1* DNA sequence, single cell transcriptomic analysis of the heart revealed subtle yet prevalent upregulation of *HAND2* and dysregulated cardiac gene expression programs. These results illustrate a crucial, fine-tuning function of the lncRNA *Hand2os1* locus in accurately controlling the spatial expression of *HAND2*, through which *Hand2os1* modulates cardiac lineage development and heart function.

The *Hand2os1* locus precisely controls *HAND2* expression

Current lines of evidence indicate that disruption of the *Hand2os1* DNA locus rather than *Hand2os1* transcription/transcripts primarily contributes to dysregulated expression of *HAND2* and heart morphological defects and lethality. The lack of discernable phenotypes in the heart and in animal survival in *Hand2os1*[P/P] mice suggests that *Hand2os1* transcripts and perhaps its transcription may be largely dispensable for cardiac development and expression of *HAND2* in the heart. Consistent with this finding, a related report showed that deletion of the first two exons of *Hand2os1* (*lncHand2*) did not cause apparent heart abnormality and failed to affect hepatic expression of *HAND2* despite the absence of *lncHand2* transcripts in mouse livers (Wang et al., 2018). Although residual transcripts were expressed in *Hand2os1*[P/P] mice (~2-7 molecules of truncated *Hand2os1*[P] transcripts per cell versus 15~40 molecules per wild-type cell) (Fig. 1C, Fig. S1C; see the Materials and Methods), the low abundance does not seem to justify a *trans* function of *Hand2os1*[P] transcripts in a broader regulation of cardiac gene programs. Our genetic evidence based on *Hand2os1*[P/P] and *Hand2os1*[F/F] mice does not support a *trans*-acting mechanism of the *Hand2os1* locus in regulating expression of cardiac genes, unless *Hand2os1* and target gene loci are in spatially close proximity in the nucleus.

For the above reasons, we conjecture that broad alterations in cardiac gene programs observed in *Hand2os1*[F/F] mutant hearts are likely to result from aberrant upregulation of *HAND2* due to the loss of *cis*-regulatory DNA sequences embedded in the *Hand2os1* locus.
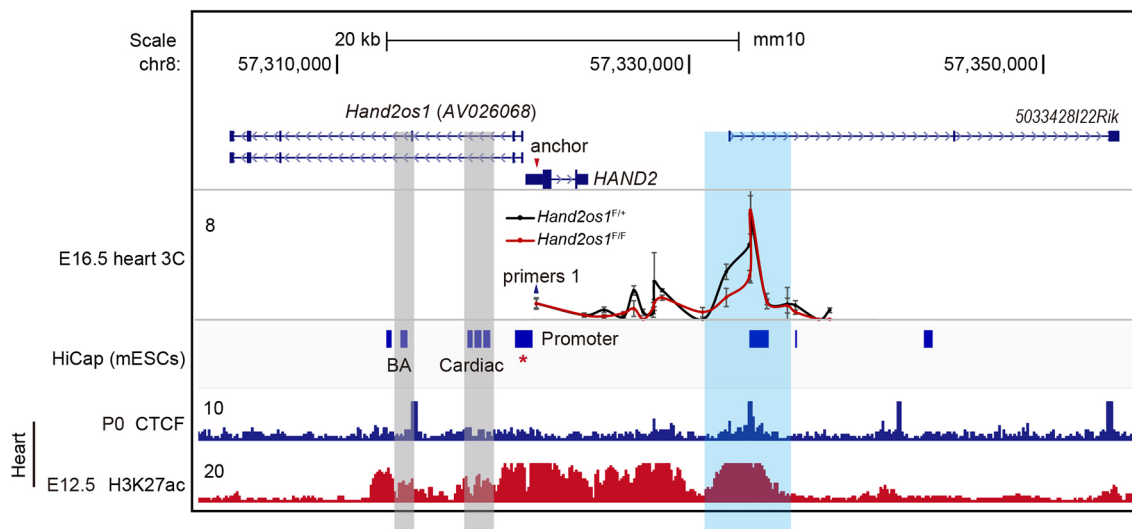
Fig. 7. *HAND2* promoter interacts with downstream enhancers in *Hand2os1*[F/F] embryonic hearts. 3C analysis in embryonic hearts at E16.5. The anchor site is indicated by a red arrowhead. The *y* axis shows interaction frequency relative to that of naked DNA control and to primers 1. Data are mean±s.e.m. (*n*=2 for each genotype). The UCSC genome browser view shows HiCap in mESCs and CTCF binding in P0 hearts, and H3K27ac in E12.5 hearts. Blue shading, putative enhancers; gray shading, the branchial arch (BA) enhancer and the cardiac enhancer; red asterisk, anchor promoter used in HiCap.

DEVELOPMENT

Hand2os1 transcripts may serve as proxy signals for the activity of important regulatory DNA elements embedded in its DNA locus in cardiac cells, in a manner similar to the lncRNA *Rroid*, the locus but not the RNA of which regulates the homoeostasis and function of specific innate lymphoid cells (Mowel et al., 2017). However, we could not absolutely exclude the possibility that the *Hand2os1* RNA might be more specifically expressed in subsets of cardiac cells, in which it regulates the expression of key cardiac genes that are genomically distal but in the chromatin neighborhood of the *Hand2os1/HAND2* locus. Other lncRNA molecules, such as *Mhrt, Wisper* and *Fendrr*, have been reported to have *trans*-acting effects on heart development and function (Grote et al., 2013; Han et al., 2014b; Micheletti et al., 2017). In addition, it remains possible that in other pathological or stress conditions yet to be revealed, *Hand2os1* transcription and transcripts may play a role in defining the chromatin environment required for the precise regulation of *HAND2* transcription.

Although the molecular effects of *Hand2os1* on *HAND2* expression in individual cells of E11.5 embryonic hearts are moderate, they can be robustly detected in hundreds of cells across all four cardiac cell types. Consistent with single cell analysis, subtle upregulation of *HAND2* was also observed in the septum and the right atrium of E16.5 *Hand2os1*[F/F] embryos. Notably, in bulk analysis of *Hand2os1*[F/F] mutant hearts, expression changes of muscle contraction genes that are distal to the *Hand2os1* locus appear to be more pronounced than changes in *HAND2* expression. Subtle *cis*-effects could be easily missed in conventional ensemble analysis, which may confound the mechanistic interpretation of the function of lncRNA in *cis* or in *trans*. Through combinational analysis of multiple mouse models and single cell characterization, we conclude that *HAND2* expression alteration is the primary molecular effect of inhibition of *Hand2os1* in heterogeneous cell populations. *HAND2* expression undergoes a decrease after E10.5 and then remains low throughout the remaining course of heart development (Srivastava et al., 1997; Tamura et al., 2014). The observed upregulation of *HAND2* in E11.5 and E16.5 *Hand2os1*[F/F] embryos may also reflect improper downregulation of *HAND2* during cardiac development.

Precise expression of *HAND2* is essential for cardiac development and function

Like many lncRNAs, such as *Flicr* and *Fendrr* (Grote et al., 2013; Zemmour et al., 2017), *Hand2os1* deletion had subtle molecular effects that nonetheless resulted in profound biological consequences *in vivo*. In *Hand2os1*[F/F] embryos, the overall formation of an organized four-chamber heart is not affected, and the morphological defects in specific regions of the heart, including lesions in the interventricular septum and ventricle hypoplasia, are moderate. However, these abnormalities in combination may be sufficient to impair heart function, as indicated by apparent blood coagulation and fatal thrombosis, thereby leading to immediate death of mutant animals upon birth.

Interestingly, single cell and bulk analysis of gene expression revealed upregulation of *HAND2* and muscle contraction genes but downregulation of septum genes in *Hand2os1*[F/F] embryos. Multiple studies using various mouse models have demonstrated that aberrantly high levels of embryonic *HAND2* led to septum lesion (Table S1). For example, *MYH7*-driven overexpression of *HAND2* prevents the formation of the interventricular septum in embryos (Togi et al., 2006). In the *Rim4* mouse model, which mimics a human chromosomal disorder caused by partial trisomy of distal 4q (4q+), a region containing 17 genes, including *HAND2*, overdose of *HAND2* has been suggested as a major cause of severe ventricular

septal defects (VSDs) and perinatal lethality (Tamura et al., 2013). In addition, mice deficient in *miRNA-1-2* express more HAND2 protein, and exhibit a VSD and embryonic death from E15.5 to just after birth with 50% penetrance (Zhao et al., 2007). Moreover, *MYH6*-driven overexpression of *HAND2* in adult cardiac muscle cells causes pathological heart hypertrophy (Dirkx et al., 2013). Comparisons of the above mouse models with the three *Hand2os1* KO mice we generated suggest a correlation between the level of *HAND2* overexpression and the severity of heart defects.

Based on these lines of evidence, we interpreted the observed molecular and morphological changes in mutant hearts to be a result of excess amounts of *HAND2* transcripts in *Hand2os1*[F/F] embryos. Our data suggest a model in which an apparently subtle but global increase in the *HAND2* dose in all cardiac cell types may alter cardiac gene programs, eventually resulting in morphological and functional abnormalities. Yet a definitive demonstration of this model will require generation of additional mouse models that overexpress *HAND2* at a level comparable with that in *Hand2os1*[F/F] mutants.

Discrepancy between the polyA KI and the full-length deletion of *Hand2os1* in mouse

Complete removal of the entire 17 kb *Hand2os1* sequence abolishes *Hand2os1* transcription and transcripts, but fails to attenuate *HAND2* expression, leading to much weaker cardiac defects and delayed onset of death, compared with *Hand2os1/Uph* polyA KI mutant embryos, which show abolished expression of *HAND2* and failed heart morphogenesis at E10.5 (Anderson et al., 2016). These discrepancies were unexpected, as polyA KI had been thought to minimally disrupt the genomic DNA compared with a large deletion. It is possible that residual low levels (~8-32%) of nascent transcription/RNA of *Hand2os1* in *Hand2os1*[P/P] embryonic hearts might have a potential effect on *HAND2* expression. Alternatively, one parsimonious explanation is that engagement of the *HAND2* promoter with downstream enhancers embedded in the lncRNA *5033428I22Rik* locus provides alternative use of enhancers that may sustain but imprecisely control *HAND2* expression in *Hand2os1*[F/F] embryonic hearts. The role of properly regulated promoter-enhancer interactions for precise gene expression has been demonstrated in the example of the lncRNA *Pvt1* (Cho et al., 2018). Another trivial interpretation is that the *Hand2os1* region might contain both negative and positive regulatory elements for *HAND2* expression (Charite et al., 2001; McFadden et al., 2000; Voth et al., 2009), and the loss of *Hand2os1* expression might be compensated by the loss of the negative element(s), of which function is normally de-repressed by the transcription of *Hand2os1*. Generation of an allelic series of deletion will define the *cis*-regulatory elements in the *Hand2os1* locus in future studies.

On the other hand, one might consider the possibility that the severe phenotypes observed in the polyA KI mice may result from polyA-induced aberrant silencing, independently of the lncRNA function. The *Hand2os1* and *HAND2* locus is bivalently marked by H3K4me3 and H3K27me3 in mesodermal precursor cells (Almada et al., 2013); and the repressive H3K27me3 mark needs to be removed prior to transcription activation of *HAND2* during the onset of cardiogenesis. Possibly, the proximal insertion of a transcription stop signal immediately upstream (−644 bp) of the *HAND2* TSS may lead to artificial recruitment of the transcription termination machinery. Given the close juxtaposition (123 bp) between the TSSs of *Hand2os1* and *HAND2*, abnormal occupancy of proteins involved in transcription termination at the proximal promoter of *HAND2* might prevent the binding of transcription activators and/or chromatin remodelers, consequently blocking the removal of

H3K27me3 and activation of *HAND2* upon heart morphogenesis. One example to support this possibility is the study of the lncRNA *ThymoD*. Insertion of a polyA signal downstream of the TSS of *ThymoD* maintains the silenced local chromatin state and inhibits its repositioning into transcriptionally active domains in the nuclear interior (Isoda et al., 2017).

Nevertheless, together with the reported polyA KI mouse model, our study clearly demonstrates the complexity of the *Hand2os1* locus in modulating *HAND2* expression. Careful examinations using more mutant animals are necessary to dissect the precise function of *Hand2os1* transcription, transcripts and its embedded DNA elements in future studies. The fact that different knockout strategies produce distinct phenotypes underlines the requirement to use complementary genetic approaches to study the physiological functions of an lncRNA in mouse models (Han et al., 2018; Luo et al., 2016; Yin et al., 2015). Last, we believe that careful genetic dissection coupled with single cell analysis will lead to in-depth understanding of the functions and mechanisms of action of lncRNAs, thus truly impacting on our understanding of the noncoding genome in animal development, fitness and disease.

MATERIALS AND METHODS

Animals
All mice we used had a C57BL/6 background, with age described in the manuscript. Embryos were isolated at the developmental stages indicated in the manuscript. All animal experiments were conducted in accordance of institutional guidelines for animal welfare and approved by the Institutional Animal Care and Use Committee (IACUC) at Tsinghua University, China.

Cells
HEK 293T cells (CRL-3216, ATCC) were cultured in DMEM supplemented with 10% heat-inactivated fetal bovine serum (Hyclone) and 1% penicillin/streptomycin (Cellgro). ESCs (46C, Austin Smith Lab) were grown in DMEM (Cellgro) supplemented with 15% heat-inactivated fetal bovine serum (Hyclone), 1% glutamax (Gibco), 1% penicillin/streptomycin (Cellgro), 1% nucleoside (Millipore), 0.1 mM 2-mercaptoethanol (Gibco), 1% MEM nonessential amino acids (Cellgro) and 1000 U/ml recombinant LIF (leukemia inhibitory factor) (Millipore) on gelatin-coated plates. All cultured cells were maintained in a humidified incubator at 37°C with 5% CO_2 (Luo et al., 2016).

CRISPR/Cas9-mediated genetic deletion
CRISPR/Cas9-mediated genetic deletion for lncRNA knockout mice generation was performed as previously described with minor modifications (Han et al., 2014a, 2018). Briefly, Cas9 mRNA and sgRNAs were co-injected into mouse zygotes. For each genetic deletion, we used two sgRNAs (*Hand2os1*[P], sg1 and sg2; *Hand2os1*[D], sg3 and sg4; *Hand2os1*[F], sg1 and sg5) (Table S10). For *Hand2os1*[P], we deleted a 1 kb DNA sequence covering the core promoter and the first two exons of *Hand2os1*, with 94% of *Hand2os1* DNA sequences remaining intact. When genetic deletion was confirmed, the germline transmission was performed for two generations by mating with C57BL/6. F2 mice and later generations were used for heterozygote intercrosses.

Genotyping
Knockout primers (forward and reverse) were designed outside of the deleted region. For wild-type band amplification, we used one of the knockout primers together with a primer designed inside of the deleted region (Table S10). Knockout bands were confirmed by Sanger sequencing (Han et al., 2018).

Echocardiography
Echocardiography was performed on *Hand2os1*[D/D], *Hand2os1*[P/P] and their littermate control mice at 6-10 weeks. Briefly, mice were gently restrained

in the investigator's hand during echocardiography detection. Two-dimensional, short-axis views of the left ventricle were obtained for guided M-mode measurements of the left ventricular (LV) internal diameter at end diastole (LVIDd) and end systole (LVIDs). LV internal diameter was measured in at least three beats from each projection and averaged. The fractional shortening (FS) was calculated by the following formula: FS (%)=[(LVIDd−LVIDs)/LVIDd]×100, which represents the relative change of left ventricular diameters during the cardiac cycle (Table S2).

Histology analyses
For Hematoxylin and Eosin staining, E16.5 embryonic hearts were fixed in 4% PFA overnight at room temperature, dehydrated through a graded ethanol series (50%, 75%, 90%, 95%, 100%) and paraffin embedded. After sectioning (7 µm), the tissues were deparaffinized in xylene and rehydrated through a graded ethanol series (100%, 95%, 75%), then stained with Hematoxylin and Eosin. Ratio of RV area was calculated as the RV chamber area divided by whole ventricle area. Thickness of RV body wall was calculated as the ventricular compact myocardial area divided by its outer circumference. Relative thickness of RV body wall was calculated as thickness of RV body wall divided by whole ventricle circumference. These data were measured in Adobe Photoshop CC2014 after selection of the image areas with myocardial color range. For immunostaining, E9.5 embryos were fixed in 4% PFA at 4°C 2 h, dehydrated by 30% sucrose and embedded in OCT. Then frozen sections was cut at 7 µm on a cryostat set at −20 to −25°C. Immunostaining was performed with primary antibodies against TNNI3 (Abcam, ab56357, 1:200) and HAND2 (Abcam, ab200040, 1:100). Primary antibodies were visualized by staining with Alexa-conjugated secondary antibodies: Alexa Fluor 488 donkey anti-goat (Life Technologies, #A-11055) and Alexa Fluor 555 donkey anti-rabbit (Life Technologies, #A-31572) diluted 1:200. All the slides were mounted in Vectashield hardset antifade mounting medium (Vector Laboratories) and imaged on a Zeiss microscope.

RNA *in situ* hybridization
Whole-mount *in situ* hybridization was carried out with digoxigenin-labelled antisense RNA probes as previously described with some modifications (Anderson et al., 2016; Wei et al., 2011). In brief, RNA probe for *HAND2* were amplified from cDNA of mouse embryonic heart and transcribed *in vitro* using T7 RNA polymerase (Roche, 10881767001) with DIG RNA labeling mix (Roche, 11277073910) (Table S10). Embryos were fixed in 4% PFA at 4°C overnight, dehydrated through a graded methanol series (50%, 75%, 100%) and stored in 100% methanol at −20°C. The embryos were bleached in a solution containing 30% H_2O_2:methanol 1:5 for 2 h, then rinsed in methanol, rehydrated through a graded methanol series (100%, 75%, 50%) and then washed in PBS. The embryos were post-fixed for 20 min in 4% PFA. After washing in PBS, embryos were transferred to the hybridization buffer (50% formamide, 5× SSC, 500 µg/ml yeast RNA, 50 µg/ml heparin and 0.1% Tween-20) and pre-hybridized for 4 h at 65°C. Hybridizations were performed in fresh hybridization buffer containing 0.25 ng/µl digoxigenin-labelled antisense RNA probes overnight at 65°C. Post-hybridization washes were performed at 65°C in wash buffer 1 (50% formamide, 2× SSC), wash buffer 2 (2× SSC) and wash buffer 3 (0.2× SSC), then performed in MABT (100 mM maleic acid, 150 mM NaCl and 0.1% Tween-20) at room temperature. After 1 h of blocking at room temperature in 10% sheep serum, 2% blocking reagent (Roche, 11096176001) (diluted in MABT), embryos were incubated overnight at 4°C in blocking solution as above, with anti-DIG-AP antibody (Roche, 11093274910, 1:3000). Then mouse embryos were washed in MABT at room temperature. After the post-antibody washes, embryos were washed in NTMT [100 mM NaCl, 100 mM Tris-HCl (pH 9.5), 50 mM MgCl2 and 0.1% Tween-20]. Staining was visualized in BM Purple AP Substrate (Roche, 11442074001).

Ink injection
Chinese ink (Yidege) was injected into the left ventricles of E16.5 embryos to visualize the organization of the arteries.

Transfection

Plasmids were transfected into 293T or ESCs using Lipofectamine 2000 (Life Technologies, #200059-61). For western blot, cells were harvested 24 h after transfection. *HAND2* cDNA with different lengths of 5′ UTR or without 5′ UTR were cloned into a *piggyBac* vector. *piggyBac*-GFP were co-transfected with *HAND2* cDNA as a control for transfection efficiency. For validation of HAND2 antibody, flag-tag was added to the N-terminal of HAND2.

Western blot

Cultured cells were washed in PBS and boiled in 5× SDS sample buffer for 5 min at 95°C. After SDS-PAGE and transfer, membranes were blocked in 5% milk/TBS-Tween. Primary antibody was applied for 2 h and secondary HRP-conjugated antibodies was applied for 1 h at room temperature. Membranes were washed for 3×10 min in TBS-Tween after each antibody incubation, and incubated with ECL substrate before exposure to X-ray film. Primary antibodies against HAND2 (Abcam, ab200040, 1:1000), β-tubulin (Abmart, M30109, 1:2000), FLAG (EASYBIO, BE2005-100, 1:2000) and GFP (CWBIO, CW0086, 1:2000) were used. Secondary antibodies used included goat anti-mouse IgG (CWBIO, CW0102) and goat anti-rabbit IgG (CWBIO, CW0103) at 1:5000 dilution.

Reverse transcription and quantitative PCR (RT-qPCR)

Tissue were washed by PBS and harvested in TRIzol reagent (Life Techonologies, #15596018). Adult cardiomyocytes were isolated using type II collagenase in the Langendorff retrograde perfusion mode (O'Connell et al., 2007). Total RNA was extracted according to the manufacture recommended procedure. Total RNA (0.5 to 2 µg) was reverse transcribed using a RevertAid First Strand cDNA Synthesis Kit (Fermentas, K1622) with random primers. RT-qPCR was performed using iTaq Universal SYBR Green Supermix (Bio-Rad, 1725121) on a Bio-Rad CFX384 or CFX96 RealTime System. RT-qPCR analysis data provide the expression relative to *GAPDH* or *18S* expression ±s.e.m. (Table S10). For the estimation of RNA molecules per cell, we first drew a standard curve to normalize the PCR efficiency of *Hand2os1* and *HAND2* RT-qPCR primers. Next, we estimated the RNA molecules per cell by normalization of counted cell number used for PCR reaction. We estimated that the abundance of *Hand2os1* transcripts is about ∼15-40 molecules per cell, relatively 7- to 23-fold lower than that of *HAND2* transcripts. In E12.5 embryonic heart and adult heart, the *Hand2os1* transcript is ∼15 and ∼40 molecules per cell, respectively (Fig. S1C). In *Hand2os1*[P/P] embryonic heart at E12.5, only 10% of truncated *Hand2os1*[P] transcripts remained, which is ∼2 molecules per cell. Similarly, in *Hand2os1*[P/P] adult heart, only ∼7 molecules per cell are detected (17% of 40 molecules) (Fig. 1C).

5′ rapid amplification of cDNA Ends (5′ RACE)

Total RNA of E16.5 hearts of *Hand2os1*[F/+] and *Hand2os1*[F/F] from heterozygotes intercrosses were used for 5′ RACE cDNA library construction. 5′ RACE was performed by following the manufacture of SMARTer RACE 5′ Kit (Clontech, 634858). One round of PCR amplification was performed with universal primer (forward) and gene-specific primer (reverse) (Table S10).

Chromatin conformation capture (3C)

E16.5 hearts of *Hand2os1*[F/+] and *Hand2os1*[F/F] from heterozygotes intercrosses were used for 3C. The 3C experiments were performed as described previously (Du et al., 2017) with minor changes. Each embryonic heart was freshly isolated and crosslinked using 1% formaldehyde. Then, the samples were lysed [10 mM Tris-HCl (pH 7.4), 10 mM NaCl, 0.1 mM EDTA, 0.5% NP-40 and proteinase inhibitor] on ice for 1 h, digested with MboI overnight, ligated at room temperature for 6 h, reverse crosslinked then their DNA was purified. The proximal ligation events were detected by RT-qPCR using the primers in Table S10. We amplified ten DNA fragments (44 kb in total) covering the *Hand2os1*/*HAND2* DNA locus we investigated as naked DNA control for 3C experiments. The interaction frequencies in embryonic hearts were normalized to that of naked DNA control.

Bulk RNA-seq and data analysis

Adult (8 week) cardiomyocytes of CTRL (*Hand2os1*^{+/+} and *Hand2os1*[D/+]) and *Hand2os1*[D/D], and E11.5 hearts and E16.5 ventricles of *Hand2os1*[F/+] and *Hand2os1*[F/F] from heterozygotes intercrosses were subjected to RNA-seq following polyA purification. The RNA libraries were constructed by following the Illumina library preparation protocols. High-throughput sequencing was performed on Illumina HiSeq 2500 or HiSeq X TEN. All RNA-seq data were mapped to the mouse reference genome (mm9) using TopHat (version 2.0.11) (Trapnell et al., 2012). Reads were assigned to their transcribed strand (Tophat parameter '–library-type=fr-firststrand'). The gene expression level was calculated using Cufflinks (version 2.0.2) (Trapnell et al., 2012) with the refFlat database from the UCSC genome browser. For visualization, the read counts were normalized by computing the numbers of reads per million of reads sequenced (RPM). Gene set enrichment analysis (GSEA) (version 2.2.4) was performed by comparing mutant samples with control samples (Subramanian et al., 2005). We used gene sets from KEGG V6.0 (Kanehisa and Goto, 2000) and gene ontology for GSEA (Table S3). First, genes with FPKM >10 and |log2 (fold change)| >0.2 [fold change=(FPKM of KO+0.1)/(FPKM of CTRL+0.1)] were selected as candidates. To exclude the inconsistently dysregulated candidates, we further filtered genes with t.test>0.1 or |log10 (t.test)×log2 (fold change)|<0.5 (dysregulation score). For 8-week-old cardiomyocytes of *Hand2os1*[D/D], 114 and 186 genes are upregulated and downregulated, respectively (Table S4). For E11.5 hearts of *Hand2os1*[F/F], 169 and 101 genes are upregulated and downregulated, respectively (Table S5). For E16.5 ventricles of *Hand2os1*[F/F], 31 and 19 genes are upregulated and downregulated, respectively (Table S6). Heatmaps were drawn using Cluster 3.0 and viewed by Treeview. The colors represent the fold change of gene expression, which is relative to average FPKM of each gene across all analyzed samples.

Single cell RNA-seq and data analysis

E11.5 hearts of wild-type and *Hand2os1*[F/F] from heterozygotes intercrosses were subjected to single cell RNA-seq. We harvested six embryonic hearts for each genotype. Embryonic hearts were trypsinized (0.25%) for 5 min at 37°C individually and subjected to fluorescence-activated cell sorting (FACS) after 7-aminoactinomycin D (AAT Bioquest, 17501) staining for collection of living single cells. Next, six embryonic hearts were combined as a single sample for 10× Genomics Single Cell 3′ library construction (10× Genomics, PN-120237). The RNA libraries were constructed by following the manufacture recommended procedure to obtain ∼5000 cells barcoded per sample. Sequencing data analyses including sample demultiplexing, barcode processing and single cell 3′ gene counting were carried out using by the Cell Ranger Single-Cell Software Suite (software.10xgenomics.com/single-cell/overview/welcome) (Zheng et al., 2017). We obtained ∼190 million reads for 3469 detected *Hand2os1*[F/F] cells and ∼181 million reads for 2563 detected wild-type cells, which indicate an average of 60,000 reads per cell. The cDNA insert was aligned to mouse reference genome (mm10). Cells with fewer than 1000 detected genes were removed. We used RandomForest approach to discriminate a population of hemopoietic cells and excluded them from downstream analysis, and finally obtained 1492 single cells from wild-type heart and 2108 single cells from *Hand2os1*[F/F] heart. On the median, we detected 3492 genes per cardiac cell. As we compared regulatory expression differences between the mutant and wild-type cardiac cells in the same heart tissue, we reasoned that sample biases towards different cell populations with various sizes and fragilities would be less pronounced in our assay. For comparative analysis of wild-type and mutant single cell datasets, we took the union of the top 1000 genes with the highest dispersion (var/mean) from both datasets ('WT' object and 'Mutant' object) to perform the alignment procedure in the Seurat integration procedure (Butler et al., 2018). We ran a canonical correlation analysis (CCA) to identify common sources of variation between the two datasets. Then we aligned the top seven CCA subspaces (or dimensionalities) to generate a single new dimensional reduction integrated WT and mutant dataset that we used for subsequent analyses such as t-SNE visualization. Next, we used the 'FindClusters' function to identify four main cardiac cell types and verified them using known marker

genes (Li et al., 2016). We achieved 43% cardiomycytes, 12% epicardial cells, 31% mesenchymal cells and 14% endothelial cells (Table S7). The dominant composition of CMs in our data is consistent with two previous single cell studies which profiled 96 cells at E11.5 and 1165 cells at E10.5 of embryonic hearts (Dong et al., 2018; Li et al., 2016). Increased percentages of MCs and EPs at E11.5 compared with those in the E10.5 heart reported previously are in accordance with increased proliferation of cushions and epicardium (Li et al., 2016). To identify unique cluster-specific marker genes and for heatmap plotting, we used the Seurat function 'FindAllMarkers' (thresh.test=0.5, test.use='roc') and define a group of differentially expressed genes (DEGs) containing 1750 genes (Table S8). Because the median UMI we detected in most of single cells did not reach one million UMIs, we used log2 (TPM/10+1) rather than log2 (TPM+1) to normalize the expression levels for following analysis. For expression analysis of *HAND2*-neighboring genes (Fig. 5D,E), a gene is defined as expressed if the corresponding transcripts are detected in more than 20% of cells in at least one cell type. Next, we identified dysregulated genes between wild-type and mutant hearts by averaged log2 (TPM/10+1) of each gene (>2) in each cell type. Genes with |log2 (mutant+1)/(wildtype+1)|>0.2 are defined as dysregulated genes, which were used for gene ontology analysis (Table S9). A total of 197 genes showed altered expression in *Hand2os1*$^{F/F}$ cardiac cells, including 56 in CMs, 120 in EPs, 54 in MCs and 80 in ECs. Correlation coefficients of cardiac cells were analyzed by 1750 DEGs. We used average gene expression of all cardiomyocytes (591 single cells) from the wild-type sample as a standard gene expression profile, and calculated the Pearson correlation of each single cell compared with the standard. GSEA was performed by comparing all single cells of *Hand2os1*$^{F/F}$ hearts with wild-type samples.

Published data collection

Published sequencing datasets used in this paper (Figs 1A and 7) were collected from Encyclopedia of DNA Elements (ENCODE) and Gene Expression Omnibus (GEO), including DHS-seq of E11.5 heart (ENCSR932SBO), CTCF ChIP-seq of postnatal day 0 (P0) heart (ENCSR491NUM), H3K27ac ChIP-seq of E12.5 heart (ENCSR123MLY), H3K4me3 ChIP-seq of E12.5 heart (ENCSR688ZOR), polyA RNA-seq of E12.5 heart (ENCSR150CUE), total RNA-seq of P0 heart (ENCSR035DLJ) (Yue et al., 2014), Pol II (8WG16) ChIP-seq of E12.5 heart (GSM1260035) (He et al., 2014), GATA4 ChIP-seq of E12.5 heart (GSM1260026) (He et al., 2014), HAND2 ChIP-seq of E10.5 heart (GSM1891956) (Laurent et al., 2017), NKX2-5 ChIP-seq of E12.5 heart (GSM1724109) (Ye et al., 2015) and HiCap in mESC (GSE60494) (Sahlén et al., 2015).

Quantification and statistical analysis

Results for RT-qPCR, echocardiography, ratio of RV area and relative thickness of RV body wall are shown as mean values with error bars representing the standard error (s.e.m.), except for *Hand2os1*/*HAND2* RT-qPCR results in cardiomyocytes from CTRL (*Hand2os1*$^{+/+,\ D/+}$) and *Hand2os1*$^{D/D}$ (shown as median with range). Replicates are indicated in the figure legends. For each comparison between two groups, statistical analysis was performed and *P*-values were calculated using an unpaired two-tailed Student's *t*-test and GraphPad Prism 5 software. Measurement of heart chamber area and circumference were performed using Adobe Photoshop CC2014. Imaging data analyses were carried out in Zen 2012. For single cell RNA-seq analyses, scatter plots (gene expression and correlation coefficient) are shown as median and interquartile range. We used a Mann–Whitney test for statistical analysis of gene expression and correlation coefficient for single cell RNA-seq results. Fisher's exact test was used for significance testing of gene expression frequency for single cell RNA-seq results. The *P*-values of Mendelian ratio are based on the χ^2 test.

Author contributions
Conceptualization: X.H., A.H., X.S.; Methodology: X.H., J.Z., Y. Liu, X.F., S.A., Y. Luo; Validation: J.Z., X.L., H.J., Y.Y.; Formal analysis: X.H., Y. Liu, X.F., H.Z.; Investigation: X.H., J.Z., S.A., S.L.; Resources: S.L., Z.C., Z.Y., F.T.; Data curation: X.H., J.Z.; Writing - original draft: X.H., J.Z., X.S.; Writing - review & editing: X.H., A.H., X.S.; Supervision: A.H., X.S.; Project administration: A.H., X.S.; Funding acquisition: A.H., X.S.

Data availability
Bulk RNA-seq and single cell RNA-seq data of embryonic or adult hearts from progenies of *Hand2os1*$^{F/+}$ or *Hand2os1*$^{D/+}$ crosses have been deposited in GEO under accession number GSE102935. Previously published datasets are listed in the Materials and Methods.

Supplementary information
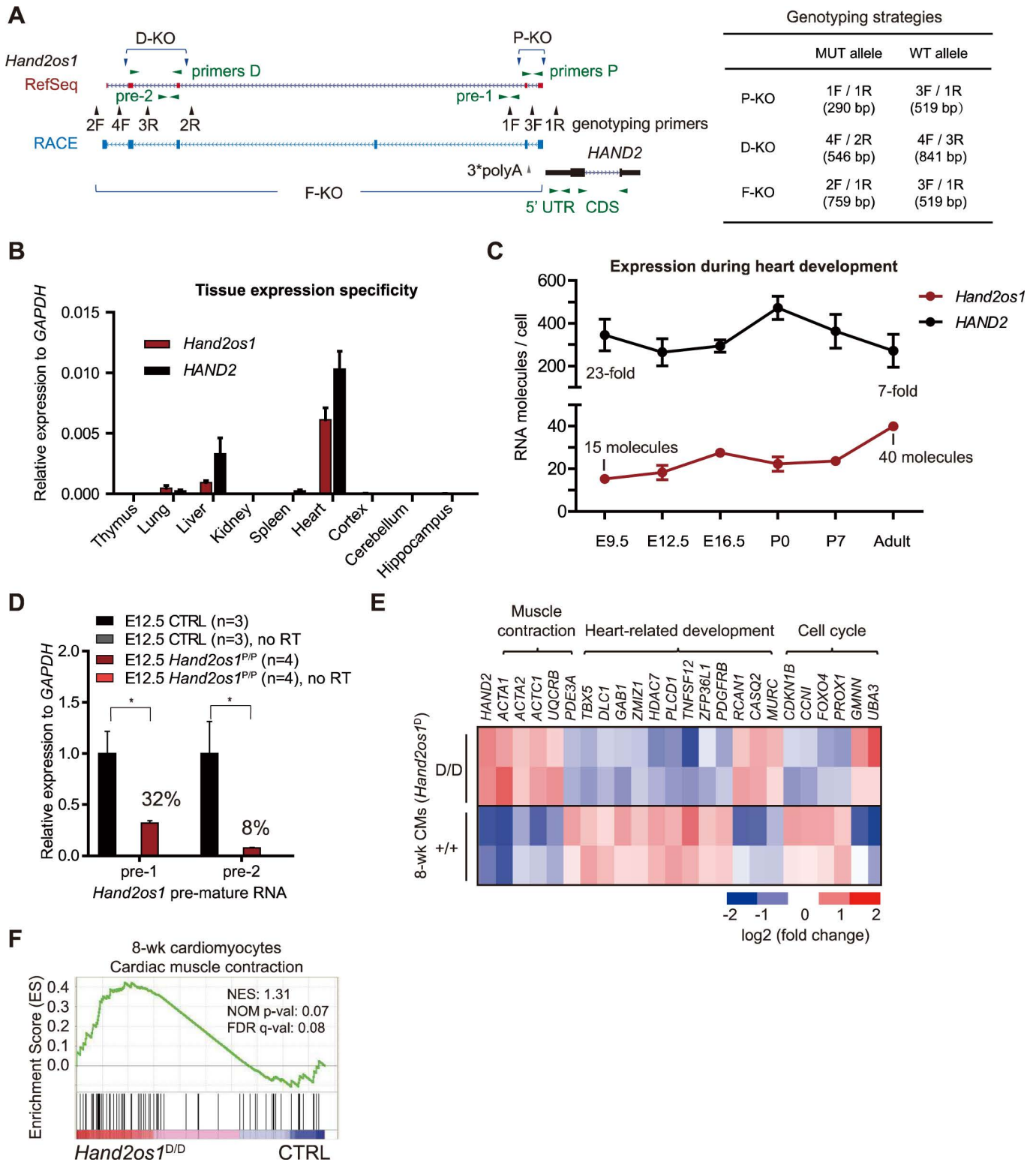Supplementary information available online at
http://dev.biologists.org/lookup/doi/10.1242/dev.176198.supplemental

References

Almada, A. E., Wu, X., Kriz, A. J., Burge, C. B. and Sharp, P. A. (2013). Promoter directionality is controlled by U1 snRNP and polyadenylation signals. *Nature* **499**, 360-363. doi:10.1038/nature12349

Anderson, K. M., Anderson, D. M., McAnally, J. R., Shelton, J. M., Bassel-Duby, R. and Olson, E. N. (2016). Transcription of the non-coding RNA upperhand controls Hand2 expression and heart development. *Nature* **539**, 433-436. doi:10.1038/nature20128

Bonev, B., Mendelson Cohen, N., Szabo, Q., Fritsch, L., Papadopoulos, G. L., Lubling, Y., Xu, X., Lv, X., Hugnot, J.-P., Tanay, A. et al. (2017). Multiscale 3D genome rewiring during mouse neural development. *Cell* **171**, 557-572.e524. doi:10.1016/j.cell.2017.09.043

Brade, T., Pane, L. S., Moretti, A., Chien, K. R. and Laugwitz, K.-L. (2013). Embryonic heart progenitors and cardiogenesis. *Cold Spring Harb. Perspect. Med.* **3**, a013847. doi:10.1101/cshperspect.a013847

Bruneau, B. G. (2005). Developmental biology: tiny brakes for a growing heart. *Nature* **436**, 181-182. doi:10.1038/436181a

Bruneau, B. G. (2008). The developmental genetics of congenital heart disease. *Nature* **451**, 943-948. doi:10.1038/nature06801

Butler, A., Hoffman, P., Smibert, P., Papalexi, E. and Satija, R. (2018). Integrating single-cell transcriptomic data across different conditions, technologies, and species. *Nat. Biotechnol.* **36**, 411-420. doi:10.1038/nbt.4096

Cai, B., Ma, W., Ding, F., Zhang, L., Huang, Q., Wang, X., Hua, B., Xu, J., Li, J., Bi, C. et al. (2018). The long noncoding RNA CAREL controls cardiac regeneration. *J. Am. Coll. Cardiol.* **72**, 534-550. doi:10.1016/j.jacc.2018.04.085

Charite, J., McFadden, D. G., Merlo, G., Levi, G., Clouthier, D. E., Yanagisawa, M., Richardson, J. A. and Olson, E. N. (2001). Role of Dlx6 in regulation of an endothelin-1-dependent, dHAND branchial arch enhancer. *Genes Dev.* **15**, 3039-3049. doi:10.1101/gad.931701

Cho, S. W., Xu, J., Sun, R., Mumbach, M. R., Carter, A. C., Chen, Y. G., Yost, K. E., Kim, J., He, J., Nevins, S. A. et al. (2018). Promoter of lncRNA gene PVT1 is a tumor-suppressor DNA boundary element. *Cell* **173**, 1398-1412.e1322. doi:10.1016/j.cell.2018.03.068

Curtis, D., Lehmann, R. and Zamore, P. D. (1995). Translational regulation in development. *Cell* **81**, 171-178. doi:10.1016/0092-8674(95)90325-9

Dirkx, E., Gladka, M. M., Philippen, L. E., Armand, A.-S., Kinet, V., Leptidis, S., El Azzouzi, H., Salic, K., Bourajjaj, M., da Silva, G. J. J. et al. (2013). Nfat and miR-25 cooperate to reactivate the transcription factor Hand2 in heart failure. *Nat. Cell Biol.* **15**, 1282-1293. doi:10.1038/ncb2866

Dong, J., Hu, Y., Fan, X., Wu, X., Mao, Y., Hu, B., Guo, H., Wen, L. and Tang, F. (2018). Single-cell RNA-seq analysis unveils a prevalent epithelial/mesenchymal hybrid state during mouse organogenesis. *Genome Biol.* **19**, 31. doi:10.1186/s13059-018-1416-2

Du, Z., Zheng, H., Huang, B., Ma, R., Wu, J., Zhang, X., He, J., Xiang, Y., Wang, Q., Li, Y. et al. (2017). Allelic reprogramming of 3D chromatin architecture during early mammalian development. *Nature* **547**, 232-235. doi:10.1038/nature23263

Grote, P., Wittler, L., Hendrix, D., Koch, F., Währisch, S., Beisaw, A., Macura, K., Bläss, G., Kellis, M., Werber, M. et al. (2013). The tissue-specific lncRNA Fendrr is an essential regulator of heart and body wall development in the mouse. *Dev. Cell* **24**, 206-214. doi:10.1016/j.devcel.2012.12.012

DEVELOPMENT

14

Han, J., Zhang, J., Chen, L., Shen, B., Zhou, J., Hu, B., Du, Y., Tate, P. H., Huang, X. and Zhang, W. (2014a). Efficient in vivo deletion of a large imprinted lncRNA by CRISPR/Cas9. RNA Biol. 11, 829-835. doi:10.4161/rna.29624

Han, P., Li, W., Lin, C.-H., Yang, J., Shang, C., Nurnberg, S. T., Jin, K. K., Xu, W., Lin, C.-Y., Lin, C.-J. et al. (2014b). A long noncoding RNA protects the heart from pathological hypertrophy. Nature 514, 102-106. doi:10.1038/nature13596

Han, X., Luo, S., Peng, G., Lu, J. Y., Cui, G., Liu, L., Yan, P., Yin, Y., Liu, W., Wang, R. et al. (2018). Mouse knockout models reveal largely dispensable but context-dependent functions of lncRNAs during development. J Mol Cell Biol 10, 175-178. doi:10.1093/jmcb/mjy003

He, A., Gu, F., Hu, Y., Ma, Q., Ye, L. Y., Akiyama, J. A., Visel, A., Pennacchio, L. A. and Pu, W. T. (2014). Dynamic GATA4 enhancers shape the chromatin landscape central to heart development and disease. Nat. Commun. 5, 4907. doi:10.1038/ncomms5907

Holler, K. L., Hendershot, T. J., Troy, S. E., Vincentz, J. W., Firulli, A. B. and Howard, M. J. (2010). Targeted deletion of Hand2 in cardiac neural crest-derived cells influences cardiac gene expression and outflow tract development. Dev. Biol. 341, 291-304. doi:10.1016/j.ydbio.2010.02.001

Isoda, T., Moore, A. J., He, Z., Chandra, V., Aida, M., Denholtz, M., Piet van Hamburg, J., Fisch, K. M., Chang, A. N., Fahl, S. P. et al. (2017). Non-coding transcription instructs chromatin folding and compartmentalization to dictate enhancer-promoter communication and T cell fate. Cell 171, 103-119.e118. doi:10.1016/j.cell.2017.09.001

Kanehisa, M. and Goto, S. (2000). KEGG: Kyoto encyclopedia of genes and genomes. Nucleic Acids Res. 28, 27-30. doi:10.1093/nar/28.1.27

Laurent, F., Girdziusaite, A., Gamart, J., Barozzi, I., Osterwalder, M., Akiyama, J. A., Lincoln, J., Lopez-Rios, J., Visel, A., Zuniga, A. et al. (2017). HAND2 target gene regulatory networks control atrioventricular canal and cardiac valve development. Cell Rep. 19, 1602-1613. doi:10.1016/j.celrep.2017.05.004

Leppek, K., Das, R. and Barna, M. (2018). Functional 5′ UTR mRNA structures in eukaryotic translation regulation and how to find them. Nat. Rev. Mol. Cell Biol. 19, 158-174. doi:10.1038/nrm.2017.103

Li, L. and Chang, H. Y. (2014). Physiological roles of long noncoding RNAs: insight from knockout mice. Trends Cell Biol. 24, 594-602. doi:10.1016/j.tcb.2014.06.003

Li, G., Xu, A., Sim, S., Priest, J. R., Tian, X., Khan, T., Quertermous, T., Zhou, B., Tsao, P. S., Quake, S. R. et al. (2016). Transcriptomic profiling maps anatomically patterned subpopulations among single embryonic cardiac cells. Dev. Cell 39, 491-507. doi:10.1016/j.devcel.2016.10.014

Luo, S., Lu, J. Y., Liu, L., Yin, Y., Chen, C., Han, X., Wu, B., Xu, R., Liu, W., Yan, P. et al. (2016). Divergent lncRNAs regulate gene expression and lineage differentiation in pluripotent cells. Cell Stem Cell 18, 637-652. doi:10.1016/j.stem.2016.01.024

McFadden, D. G., Charite, J., Richardson, J. A., Srivastava, D., Firulli, A. B. and Olson, E. N. (2000). A GATA-dependent right ventricular enhancer controls dHAND transcription in the developing heart. Development 127, 5331-5341.

McFadden, D. G., Barbosa, A. C., Richardson, J. A., Schneider, M. D., Srivastava, D. and Olson, E. N. (2005). The Hand1 and Hand2 transcription factors regulate expansion of the embryonic cardiac ventricles in a gene dosage-dependent manner. Development 132, 189-201. doi:10.1242/dev.01562

Micheletti, R., Plaisance, I., Abraham, B. J., Sarre, A., Ting, C. C., Alexanian, M., Maric, D., Maison, D., Nemir, M., Young, R. A. et al. (2017). The long noncoding RNA Wisper controls cardiac fibrosis and remodeling. Sci Transl Med 9. doi:10.1126/scitranslmed.aai9118

Morikawa, Y. and Cserjesi, P. (2008). Cardiac neural crest expression of Hand2 regulates outflow and second heart field development. Circ. Res. 103, 1422-1429. doi:10.1161/CIRCRESAHA.108.180083

Morikawa, Y., D'Autréaux, F., Gershon, M. D. and Cserjesi, P. (2007). Hand2 determines the noradrenergic phenotype in the mouse sympathetic nervous system. Dev. Biol. 307, 114-126. doi:10.1016/j.ydbio.2007.04.027

Morris, K. V. and Mattick, J. S. (2014). The rise of regulatory RNA. Nat. Rev. Genet. 15, 423-437. doi:10.1038/nrg3722

Mowel, W. K., McCright, S. J., Kotzin, J. J., Collet, M. A., Uyar, A., Chen, X., DeLaney, A., Spencer, S. P., Virtue, A. T., Yang, E. et al. (2017). Group 1 innate lymphoid cell lineage identity is determined by a cis-regulatory element marked by a long non-coding RNA. Immunity 47, 435-449.e438. doi:10.1016/j.immuni.2017.08.012

O'Connell, T. D., Rodrigo, M. C. and Simpson, P. C. (2007). Isolation and culture of adult mouse cardiac myocytes. Methods Mol. Biol. 357, 271-296. doi:10.1385/1-59745-214-9:271

Olson, E. N. and Schneider, M. D. (2003). Sizing up the heart: development redux in disease. Genes Dev. 17, 1937-1956. doi:10.1101/gad.1110103

Osterwalder, M., Barozzi, I., Tissières, V., Fukuda-Yuzawa, Y., Mannion, B. J., Afzal, S. Y., Lee, E. A., Zhu, Y., Plajzer-Frick, I., Pickle, C. S. et al. (2018). Enhancer redundancy provides phenotypic robustness in mammalian development. Nature 554, 239-243. doi:10.1038/nature25461

Pauli, A., Rinn, J. L. and Schier, A. F. (2011). Non-coding RNAs as regulators of embryogenesis. Nat. Rev. Genet. 12, 136-149. doi:10.1038/nrg2904

Ponjavic, J., Oliver, P. L., Lunter, G. and Ponting, C. P. (2009). Genomic and transcriptional co-localization of protein-coding and long non-coding RNA pairs in the developing brain. PLoS Genet. 5, e1000617. doi:10.1371/journal.pgen.1000617

Sahlén, P., Abdullayev, I., Ramsköld, D., Matskova, L., Rilakovic, N., Lötstedt, B., Albert, T. J., Lundeberg, J. and Sandberg, R. (2015). Genome-wide mapping of promoter-anchored interactions with close to single-enhancer resolution. Genome Biol. 16, 156. doi:10.1186/s13059-015-0727-9

Shao, M., Chen, G., Lv, F., Liu, Y., Tian, H., Tao, R., Jiang, R., Zhang, W. and Zhuo, C. (2017). LncRNA TINCR attenuates cardiac hypertrophy by epigenetically silencing CaMKII. Oncotarget 8, 47565-47573. doi:10.18632/oncotarget.17735

Song, K., Nam, Y.-J., Luo, X., Qi, X., Tan, W., Huang, G. N., Acharya, A., Smith, C. L., Tallquist, M. D., Neilson, E. G. et al. (2012). Heart repair by reprogramming non-myocytes with cardiac transcription factors. Nature 485, 599-604. doi:10.1038/nature11139

Srivastava, D., Thomas, T., Lin, Q., Kirby, M. L., Brown, D. and Olson, E. N. (1997). Regulation of cardiac mesodermal and neural crest development by the bHLH transcription factor, dHAND. Nat. Genet. 16, 154-160. doi:10.1038/ng0697-154

Subramanian, A., Tamayo, P., Mootha, V. K., Mukherjee, S., Ebert, B. L., Gillette, M. A., Paulovich, A., Pomeroy, S. L., Golub, T. R., Lander, E. S. et al. (2005). Gene set enrichment analysis: a knowledge-based approach for interpreting genome-wide expression profiles. Proc. Natl. Acad. Sci. USA 102, 15545-15550. doi:10.1073/pnas.0506580102

Tamura, M., Hosoya, M., Fujita, M., Iida, T., Amano, T., Maeno, A., Kataoka, T., Otsuka, T., Tanaka, S., Tomizawa, S. et al. (2013). Overdosage of Hand2 causes limb and heart defects in the human chromosomal disorder partial trisomy distal 4q. Hum. Mol. Genet. 22, 2471-2481. doi:10.1093/hmg/ddt099

Tamura, M., Amano, T. and Shiroishi, T. (2014). The Hand2 gene dosage effect in developmental defects and human congenital disorders. Curr. Top. Dev. Biol. 110, 129-152. doi:10.1016/B978-0-12-405943-6.00003-8

Togi, K., Yoshida, Y., Matsumae, H., Nakashima, Y., Kita, T. and Tanaka, M. (2006). Essential role of Hand2 in interventricular septum formation and trabeculation during cardiac development. Biochem. Biophys. Res. Commun. 343, 144-151. doi:10.1016/j.bbrc.2006.02.122

Trapnell, C., Roberts, A., Goff, L., Pertea, G., Kim, D., Kelley, D. R., Pimentel, H., Salzberg, S. L., Rinn, J. L. and Pachter, L. (2012). Differential gene and transcript expression analysis of RNA-seq experiments with TopHat and Cufflinks. Nat. Protoc. 7, 562-578. doi:10.1038/nprot.2012.016

Tsuchihashi, T., Maeda, J., Shin, C. H., Ivey, K. N., Black, B. L., Olson, E. N., Yamagishi, H. and Srivastava, D. (2011). Hand2 function in second heart field progenitors is essential for cardiogenesis. Dev. Biol. 351, 62-69. doi:10.1016/j.ydbio.2010.12.023

VanDusen, N. J. and Firulli, A. B. (2012). Twist factor regulation of non-cardiomyocyte cell lineages in the developing heart. Differentiation 84, 79-88. doi:10.1016/j.diff.2012.03.002

VanDusen, N. J., Casanovas, J., Vincentz, J. W., Firulli, B. A., Osterwalder, M., Lopez-Rios, J., Zeller, R., Zhou, B., Grego-Bessa, J., De La Pompa, J. L. et al. (2014). Hand2 is an essential regulator for two Notch-dependent functions within the embryonic endocardium. Cell Rep. 9, 2071-2083. doi:10.1016/j.celrep.2014.11.021

Viereck, J., Kumarswamy, R., Foinquinos, A., Xiao, K., Avramopoulos, P., Kunz, M., Dittrich, M., Maetzig, T., Zimmer, K., Remke, J. et al. (2016). Long noncoding RNA Chast promotes cardiac remodeling. Sci. Transl. Med. 8, 326ra322. doi:10.1126/scitranslmed.aaf1475

Voth, H., Oberthuer, A., Simon, T., Kahlert, Y., Berthold, F. and Fischer, M. (2009). Co-regulated expression of HAND2 and DEIN by a bidirectional promoter with asymmetrical activity in neuroblastoma. BMC Mol. Biol. 10, 28. doi:10.1186/1471-2199-10-28

Wang, Y., Zhu, P., Wang, J., Zhu, X., Luo, J., Meng, S., Wu, J., Ye, B., He, L., Du, Y. et al. (2018). Long noncoding RNA lncHand2 promotes liver repopulation via c-Met signaling. J. Hepatol. 69, 861-872. doi:10.1016/j.jhep.2018.03.029

Wei, Q., Manley, N. R. and Condie, B. G. (2011). Whole mount in situ hybridization of E8.5 to E11.5 mouse embryos. J. Vis. Exp.

Yanagisawa, H., Clouthier, D. E., Richardson, J. A., Charité, J. and Olson, E. N. (2003). Targeted deletion of a branchial arch-specific enhancer reveals a role of dHAND in craniofacial development. Development 130, 1069-1078. doi:10.1242/dev.00337

Ye, W., Wang, J., Song, Y., Yu, D., Sun, C., Liu, C., Chen, F., Zhang, Y., Wang, F., Harvey, R. P. et al. (2015). A common Shox2-Nkx2-5 antagonistic mechanism primes the pacemaker cell fate in the pulmonary vein myocardium and sinoatrial node. Development 142, 2521-2532. doi:10.1242/dev.120220

Yin, Y., Yan, P., Lu, J., Song, G., Zhu, Y., Li, Z., Zhao, Y., Shen, B., Huang, X., Zhu, H. et al. (2015). Opposing roles for the lncRNA haunt and its genomic locus in regulating HOXA gene activation during embryonic stem cell differentiation. Cell Stem Cell 16, 504-516. doi:10.1016/j.stem.2015.03.007

Yue, F., Cheng, Y., Breschi, A., Vierstra, J., Wu, W., Ryba, T., Sandstrom, R., Ma, Z., Davis, C., Pope, B. D. et al. (2014). A comparative encyclopedia of DNA elements in the mouse genome. Nature 515, 355-364. doi:10.1038/nature13992

Zemmour, D., Pratama, A., Loughhead, S. M., Mathis, D. and Benoist, C. (2017). Flicr, a long noncoding RNA, modulates Foxp3 expression and

autoimmunity. *Proc. Natl. Acad. Sci. USA* **114**, E3472-E3480. doi:10.1073/pnas.1700946114

Zhao, Y., Samal, E. and Srivastava, D. (2005). Serum response factor regulates a muscle-specific microRNA that targets Hand2 during cardiogenesis. *Nature* **436**, 214-220. doi:10.1038/nature03817

Zhao, Y., Ransom, J. F., Li, A., Vedantham, V., von Drehle, M., Muth, A. N., Tsuchihashi, T., McManus, M. T., Schwartz, R. J. and Srivastava, D. (2007).

Dysregulation of cardiogenesis, cardiac conduction, and cell cycle in mice lacking miRNA-1-2. *Cell* **129**, 303-317. doi:10.1016/j.cell.2007.03.030

Zheng, G. X. Y., Terry, J. M., Belgrader, P., Ryvkin, P., Bent, Z. W., Wilson, R., Ziraldo, S. B., Wheeler, T. D., McDermott, G. P., Zhu, J. et al. (2017). Massively parallel digital transcriptional profiling of single cells. *Nat. Commun.* **8**, 14049. doi:10.1038/ncomms14049

A

Genotyping strategies

	MUT allele	WT allele
P-KO	1F / 1R (290 bp)	3F / 1R (519 bp)
D-KO	4F / 2R (546 bp)	4F / 3R (841 bp)
F-KO	2F / 1R (759 bp)	3F / 1R (519 bp)

B Tissue expression specificity

C Expression during heart development

D

E

F 8-wk cardiomyocytes Cardiac muscle contraction

NES: 1.31
NOM p-val: 0.07
FDR q-val: 0.08

**Fig. S1. Genetic and survival characterization of *Hand2os1* KO mice**

(A) *Hand2os1* and *HAND2* primers for RT-qPCR are shown with horizontal green arrowheads. In *Hand2os1*, primers P and D are located within the proximal and distal deletions, respectively. In *HAND2*, primers 5' UTR are located in the first 500 bp of *HAND2* mRNA, and primers CDS flank the CDS region in exon 1 and exon 2. Genotyping primers for the three *Hand2os1* KO lines are shown with vertical black arrowheads. The three deletion alleles were characterized by PCR with different combinations of genotyping primers, as shown in the right panel. (B) RT-qPCR analysis of *HAND2* and *Hand2os1* expression (primers D) across the indicated tissues in adult mouse (8-weeks old). The y axis shows expression relative to *GAPDH*. Data are shown as mean ± s.e.m.. (C) Analysis of transcript abundance of *HAND2* and *Hand2os1* by RT-qPCR in the bulk heart from the embryonic stage E9.5 to the adult (8-wk). *Hand2os1* RT-qPCR used primers D. The y axis shows relative numbers of RNA molecules per cell. Data are shown as mean ± s.e.m.. The abundance of transcripts per cell was estimated by normalizing *HAND2* and *Hand2os1* PCR signals to primer-specific PCR efficiency and the numbers of cells used for RT-qPCR and to *18S* rRNA. In embryos, cardiac expression of *Hand2os1* continues to rise, while that of *HAND2* decreases from E9.5 to E16.5. Similarly, after birth, *Hand2os1* shows significantly increased expression from postnatal day P0 to adult (8-wk), while *HAND2* expression appears to be slightly decreased. The abundance of *Hand2os1* transcripts is about 7- to 23-fold lower than that of *HAND2* in the time course analyzed. (D) RT-qPCR analysis of *Hand2os1* pre-mature RNA in E12.5 hearts from the control (CTRL, wild-type and heterozygote littermates) and *Hand2os1*$^{P/P}$ mice. No signal was detected in samples without reverse transcriptase (no RT) in RT-qPCR. The pair of primers 'pre-1' locate at 5' end of *Hand2os1* intron 2. The pair of primers 'pre-2' locate within the exon 4 and intron 4 of *Hand2os1* (panel A). 3' end of *Hand2os1* pre-mature RNA showed a more dramatic downregulation compared to 5' end. These results indicate residual transcription of *Hand2os1* in *Hand2os1*$^{P/P}$ mutant hearts. The y axis shows expression relative to *GAPDH* (normalized to CTRL). Data are shown as mean ± s.e.m.. *, p<0.05. n, number of analyzed mice. (E) Heatmap shows representative genes that are dysregulated in 8-wk cardiomyocytes of *Hand2os1*$^{D/D}$ (rep1 and rep2) compared to wild-type (rep1 and rep2) littermates (n=2). Genes shown are involved in muscle contraction, heart-related development and cell cycle. The colored bar indicates log2 (fold change over average FPKM of each gene across 4 samples). Other samples that are not in the same litter are not considered. (F) GSEA of 8-wk cardiomyocytes from CTRL (wild-type and heterozygote littermates) (n=7) and *Hand2os1*$^{D/D}$ (n=6) mice. Enrichment plot shows that genes related to cardiac muscle contraction (KEGG PATHWAY: mmu04260) are upregulated in *Hand2os1*$^{D/D}$ mice compared to controls. NES, normalized enrichment Score.

A

B

C

D

E
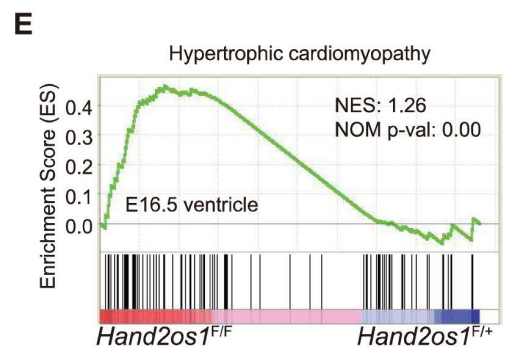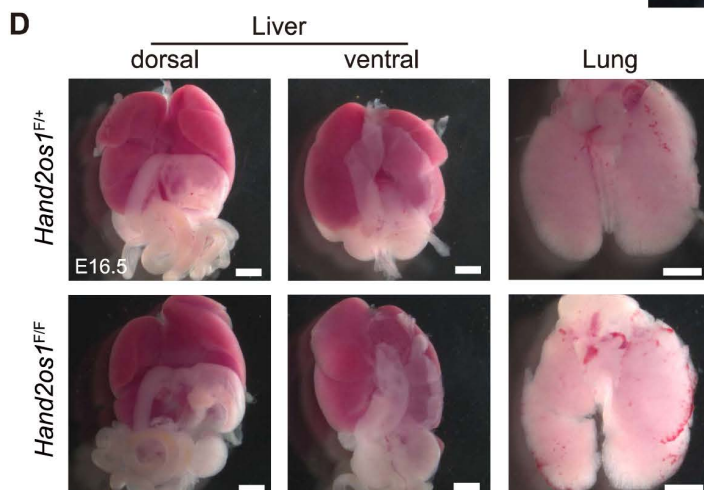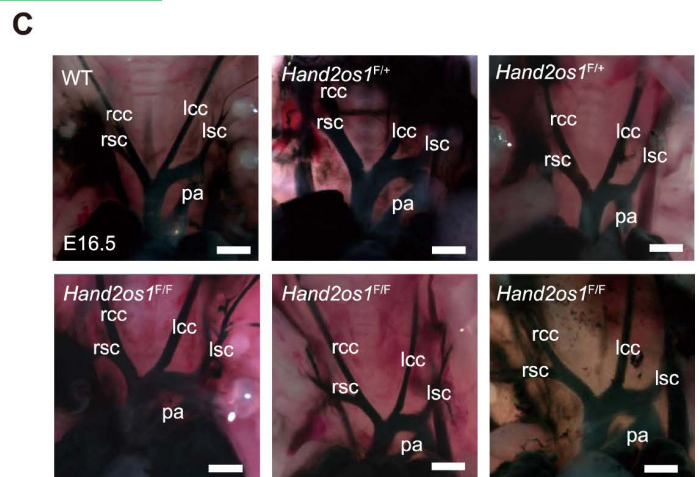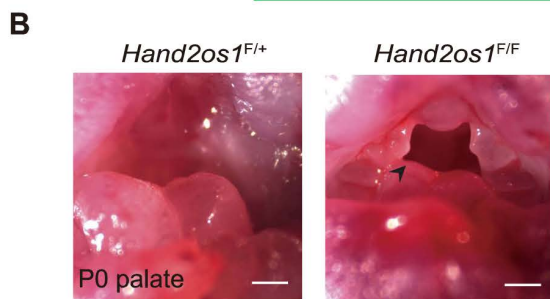
Fig. S2. Morphological characterization of *Hand2os1*^{F/F} embryos

(A) The genome browser view shows expression (strand-specific polyA RNA-seq signal) of *Hand2os1* and *HAND2* in E11.5 hearts (top) and E16.5 ventricles (bottom) from *Hand2os1*^{F/F} mutants compared to *Hand2os1*^{F/+} littermates (n=3 for each genotype). The yellow shadings indicate *Hand2os1*^{F/F} mutants. The green boxes indicate *Hand2os1* expression signal. (B) Gross morphological analysis of P0 palate of *Hand2os1*^{F/+} and *Hand2os1*^{F/F} mice reveals craniofacial defects (arrowhead) in *Hand2os1*^{F/F} newborns. A suckling defect is not the cause of death in *Hand2os1*^{F/F} pups, as these animals die within hours after birth. Mice lacking the branchial arch enhancer have craniofacial defects and cannot suckle, and die with an empty stomach 24 hours after birth. Scale bar, 500 μm. (C) Vasculature visualization by Chinese ink injection into the left ventricle of *Hand2os1*^{F/F} and CTRL (*Hand2os1*^{+/+} and *Hand2os1*^{F/+}) embryos at E16.5. lcc, left common carotid artery; lsc, left subclavian artery; pa, pulmonary artery; rcc, right common carotid artery; rsc, right subclavian artery. Scale bar, 500 μm. (D) Gross morphological examination of liver and lung of *Hand2os1*^{F/+} and *Hand2os1*^{F/F} embryos at E16.5. Scale bar, 1000 μm. (E) GSEA of E16.5 ventricles of *Hand2os1*^{F/+} and *Hand2os1*^{F/F} mice (n=3 for each genotype). Enrichment plot shows that genes related to hypertrophic cardiomyopathy (KEGG PATHWAY: mmu05410) are upregulated in *Hand2os1*^{F/F} mice compared to *Hand2os1*^{F/+} controls.
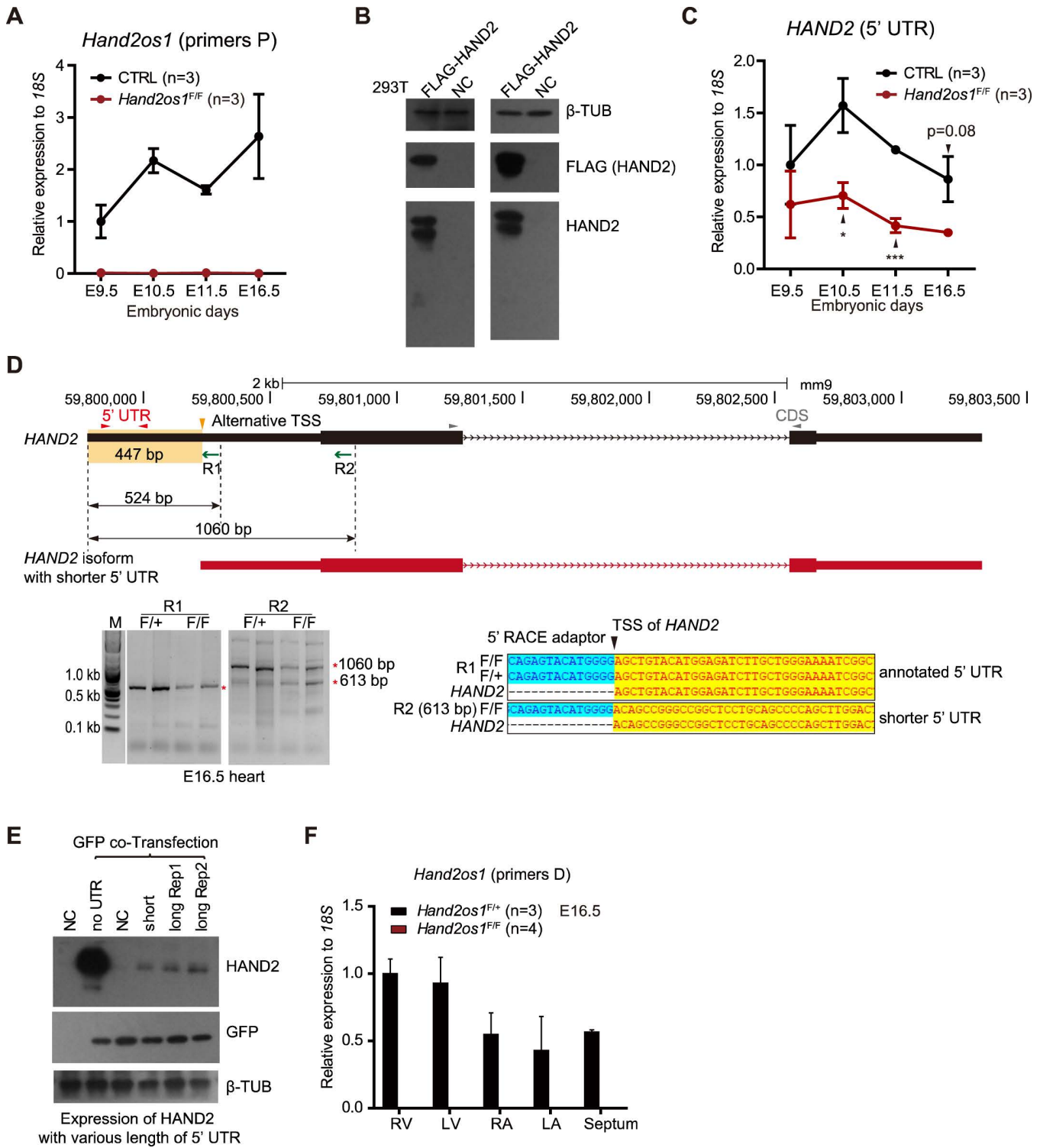
Fig. S3. Molecular analysis of *Hand2os1*$^{F/F}$ embryos

(A) RT-qPCR analysis of *Hand2os1* (primers P) in embryonic hearts at various stages from CTRL (*Hand2os1*$^{+/+, F/+}$) and *Hand2os1*$^{F/F}$. The y axis shows expression relative to *18S* (normalized to *Hand2os1* expression in CTRL embryos at E9.5). Data are shown as mean ± s.e.m..

(B) Western blot validation of the HAND2 antibody in 293T cells transfected with Flag-HAND2. β-TUBULIN is the loading control.

(C) RT-qPCR analysis of *HAND2* (5' UTR) in embryonic hearts at various stages from CTRL (*Hand2os1*$^{+/+, F/+}$) and *Hand2os1*$^{F/F}$. The y axis shows expression relative to *18S* (normalized to *HAND2* 5' UTR expression in CTRL embryos at E9.5). Data are shown as mean ± s.e.m.. *, p<0.05; ***, p<0.001.

(D) Strategy for *HAND2* 5' RACE is shown. R1 and R2, gene specific primers for 5' RACE PCR amplification, are shown together with length of their PCR products. Annotated and shorter *HAND2* isoforms are indicated in black and red, respectively. Left, DNA gel of 5' RACE PCR products. *HAND2* specific PCR bands are indicated by red asterisks. Right, Sanger sequencing results of *HAND2* 5' end revealed by 5' RACE PCR. 5' RACE analysis revealed an alternative TSS of *HAND2*, which is 447 bp downstream to the annotated TSS and 477 bp prior to CDS of *HAND2*.

(E) Western blot shows HAND2 expression from constructs with various lengths of *HAND2* 5'UTR or without the 5'UTR. Transfections were performed in mouse ESCs. β-TUBULIN is the loading control and GFP is the transfection control.

(F) RT-qPCR analysis of *Hand2os1* (primers D) in dissected E16.5 embryonic hearts (RV, LV, RA, LA and septum) from *Hand2os1*$^{F/+}$ and *Hand2os1*$^{F/F}$. The y axis shows expression relative to *18S* (normalized to *Hand2os1* expression in RV of *Hand2os1*$^{F/+}$ embryos). Data are shown as mean ± s.e.m..

n, number of analyzed mice.
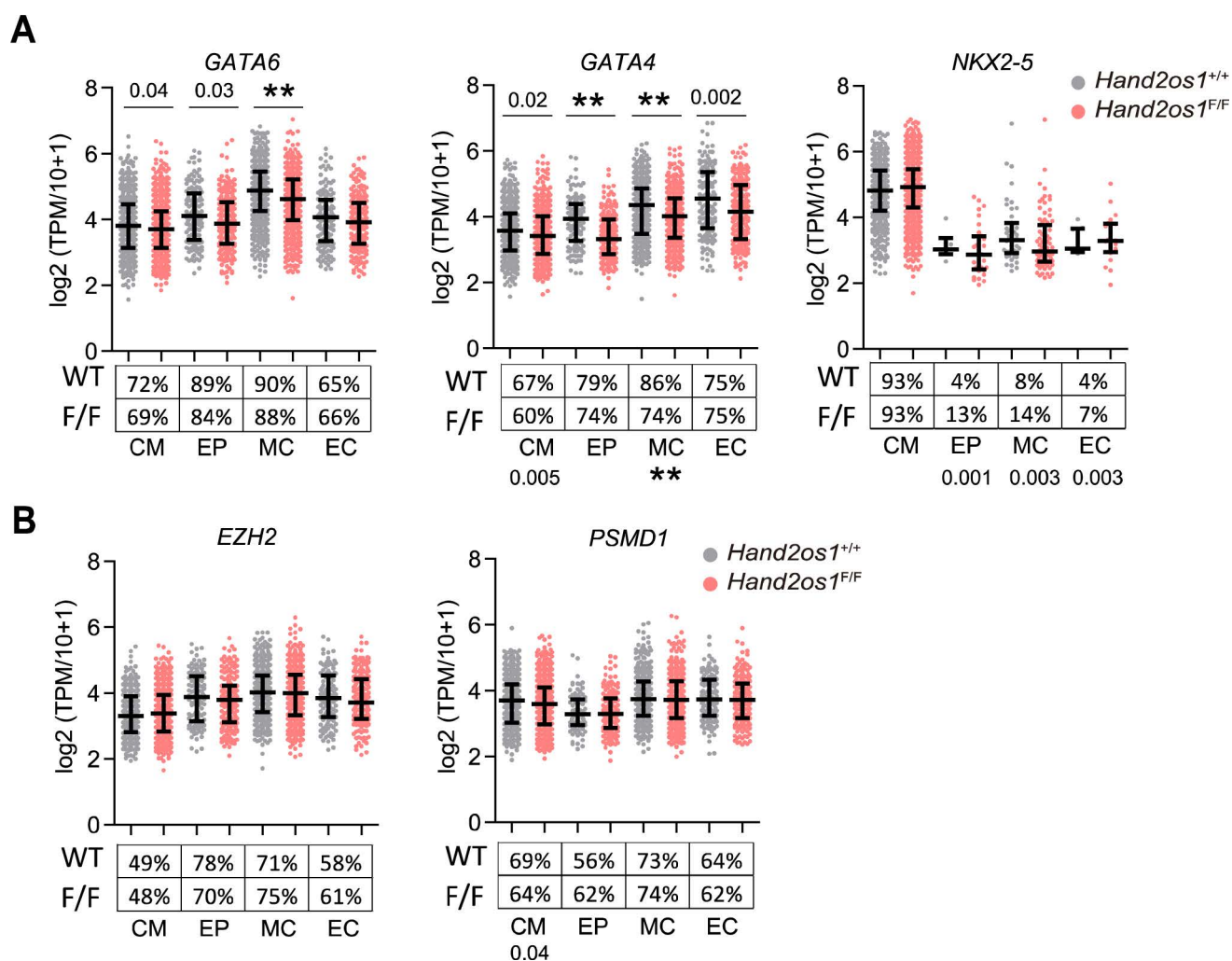
Fig. S4. Gene expression in *Hand2os1*^F/F embryos

(A-B) Scatter plots show expression level and frequency of *GATA6*, *GATA4* and *NKX2-5* (A), and *EZH2* and *PSMD1* (B) in cardiac cells of *Hand2os1*^F/F and wild-type embryonic hearts. Data are shown as median and interquartile range. The *p*-values are indicated: $0.0001 < p < 0.05$; **, $p < 0.0001$. The percentages of expressing cells (TPM>0) in each cell type are shown under the plots.
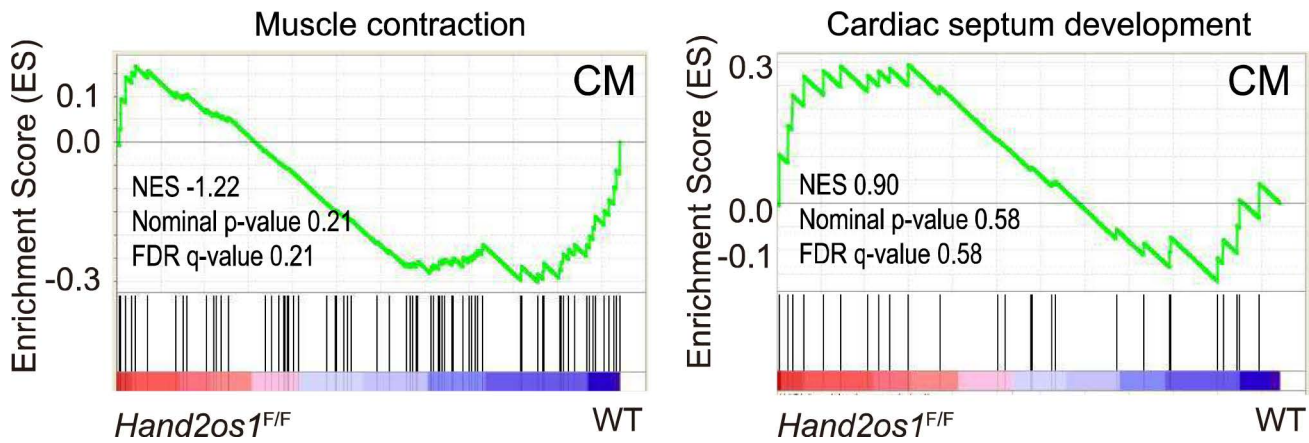
Fig. S5. Aberrant cardiac gene programs in *Hand2os1*$^{F/F}$ embryos

Non-significant changes of genes related to muscle contraction (GO: 0006936) and cardiac septum development (GO: 0003279) in CMs of *Hand2os1*$^{F/F}$ versus wild-type E11.5 hearts by GSEA.

Table S1. Summary for cardiac *HAND2* knockout/overexpression mouse models

KO/OE strategy		Loss/gain of *HAND2* expression	Phenotype
Synthetic KO		complete loss	failed right ventricle formation and lethality at E10.5
Conditional KO (*cre*)	*ISLET1*	early SHF cells	phenocopying *HAND2* synthetic KO hearts
	CTNT	myocardium	lethality at E12.5, with a single clearly defined ventricle
	NKX2-5	RV and LV chambers after E8.5	heart formed, slightly smaller RV and LV at E9.5 and lethality at E12.5
	WNT1	neural crest-derived cells	die at E12.5 with severe cardiovascular and facial defects; embryos survived to later stages with drugs, misalignment of OFT and aortic arch arteries, DORV with a membranous VSD
	MEF2C	a subset of the SHF-derived cells (OFT and RV, IVS)	smaller RV at E9.5 and a hypoplastic RV with thinner myocardium, lacking the anlage of a tricuspid valve and displaying VSDs at E12.5, lethality at E13.5
	TIE2	endothelial cells from E8.5	no patent tricuspid valve, with IVS defects, and hypotrabeculated ventricles, lethality at E14.5
	NFATC1	endocardium from E9.0	defects in trabeculation, malformed IVS and atresia, large protrusions of myocardium and multiple IVSs
	TBX1	distal OFT and pulmonary artery	a shortened OFT with normal RV at E10.5, smaller RV and outflow tracts by E13.5, lethality at E15.5
Transgenic OE	*MYH7*	whole ventricles of embryo	complete absence of the IVS
	MYH6	postnatal myocardium	pathological hypertrophy
Chromosome duplication	*RIM4*	severe VSD (80%), perinatal lethality (80%)	
miRNA-1-2 KO		4-fold increased at protein level	VSD(50%), perinatal death with 50% lethality by weaning.

SHF, second heart field; OFT, outflow tract; RV, right ventricle; IVS, interventricular septum; VSD, ventricular septal defect; DORV, double outlet right ventricle

Synthetic KO (Srivastava et al., 1997); Conditional KO with specific promoter-*cre* (*ISLET1* (Tsuchihashi et al., 2011), *CTNT* (Morikawa and Cserjesi, 2008), *NKX2-5* (Tsuchihashi et al., 2011), *WNT1* (Holler et al., 2010; Morikawa and Cserjesi, 2008; Morikawa et al., 2007), *MEF2C* (Tsuchihashi et al., 2011), *TIE2* (VanDusen et al., 2014), *NFATC1* (VanDusen et al., 2014), *TBX1* (Tsuchihashi et al., 2011)); Transgenic OE (*MYH7* (Dirkx et al., 2013), *MYH6* (Togi et al., 2006)); Chromosome duplication (Tamura et al., 2013); *miRNA-1-2* KO (Zhao et al., 2007)

Table S2. Echocardiography data of *Hand2os1*^{D/D} and *Hand2os1*^{P/P} mice

Click here to Download Table S2

Table S3. Gene sets for GSEA

Click here to Download Table S3

Table S4. Dysregulated genes in 8-wk cardiomyocytes of *Hand2os1*^{D/D} mice

Click here to Download Table S4

Table S5. Dysregulated genes in E11.5 hearts of *Hand2os1*^{F/F} embryos

Click here to Download Table S5

Table S6. Dysregulated genes in E16.5 ventricles of *Hand2os1*^{F/F} embryos

Click here to Download Table S6

Table S7. Single-cell clustering

Click here to Download Table S7

Table S8. 1750 differentially expressed genes in four types of cardiac cells

Click here to Download Table S8

Table S9. Dysregulated genes in four cardiac cell types in E11.5 hearts of *Hand2os1*$^{F/F}$ embryos

Click here to Download Table S9

Table S10. Oligos (sgRNAs, genotyping primers, RT-qPCR primers, ISH probe, 5' RACE primers, 3C primers)

Click here to Download Table S10